Eur. J. Mineral., 35, 1–24, 2023
https://doi.org/10.5194/ejm-35-1-2023

European Journal of Mineralogy
Open Access

Research article

Reactive interaction between migmatite-related melt and mafic rocks: clues from the Variscan lower crust of Palmi (southwestern Calabria, Italy)

Maria Rosaria Renna

Dipartimento di Scienze Matematiche e Informatiche, Scienze Fisiche e Scienze della Terra, Università degli Studi di Messina, Messina, Italy

Correspondence: Maria Rosaria Renna (mrenna@unime.it)

Received: 26 May 2022 – Accepted: 19 November 2022 – Published: 4 January 2023

Abstract. In the Variscan lower–intermediate crust exposed in the Palmi area (southwestern Calabria, Italy), amphibolites occur as foliated, decimeter-thick layers within migmatitic paragneiss and as a decametric main body adjacent to the migmatites. The main body is mostly fine-grained and weakly to moderately foliated; unfoliated medium-grained portions rarely occur. Amphibolites are mainly composed of plagioclase (An_{80-91}) frequently developing triple junctions, amphibole consisting of cummingtonite rimmed by hornblende and variable amounts of biotite. Minor quartz is present in amphibolite layers within paragneiss. Accessory allanite occurs in amphibolite layers within migmatites and in foliated, fine-grained portions from the main body. This study mainly aims to achieve information about the effects triggered by the migration of migmatite-related melts into associated mafic rocks and its role in the re-distribution of major and trace elements out of the anatectic source.

On the basis of whole-rock major- and trace-element compositions, the protolith of amphibolite is recognized as of cumulus origin, likely derived from basic melt emplaced in the framework of the late-Variscan lithospheric extension. The rocks experienced high-temperature subsolidus re-equilibration ($\sim$ 800 °C) in conjunction with the development of amphibole. The origin of amphibole is attributed to a coupled dissolution–precipitation process related to the reaction between migrating SiO_2-rich hydrous melt and precursor orthopyroxene ($\pm$ plagioclase). Reactive melt migration also caused the crystallization of biotite $\pm$ allanite $\pm$ quartz $\pm$ plagioclase. SiO_2-rich hydrous melt had REE (rare earth element) compositions similar to late-Variscan peraluminous granites and could have been derived by partial melting of metasediments akin to neighboring migmatitic paragneisses.

Both whole-rock and amphibole analyses reveal a decrease in Mg# ($Mg/(Mg + Fe^{2+})$) from amphibolite layers within paragneiss to fine- and medium-grained rocks of the main body. Hornblende shows an increase in SiO_2 and a decrease in Al_2O_3 and K_2O with increasing Mg#. Amphibolites interlayered with paragneiss have higher K_2O, Rb, Ba, Th, U and Zr relative to those from the main body. Furthermore, amphibole from amphibolites interlayered with paragneiss is distinct for relatively high Rb, Ba, MREE (middle rare earth element) and HREE (heavy rare earth element) concentrations. Within the main body, foliated, fine-grained rock has both the whole rock and amphibole enriched in Rb and Ba and high Zr bulk-rock contents. Whole-rock and mineral chemistry heterogeneity most likely reflects (i) variation of the composition of the melt during its reactive migration, in response to dissolution of pre-existing minerals and crystallization of new phases, and (ii) variable modification of the original compositions. Foliated and fine-grained amphibolites record the strongest modification, thereby suggesting that they represent permeable pathway enabling effective interaction of the reacting melt with precursor minerals and nucleation of new mineral phases.

Published by Copernicus Publications on behalf of the European mineralogical societies DMG, SEM, SIMP & SFMC.

1 Introduction

Partial melting and felsic-melt movement from the sites of generation in the lower crust to sites of accumulation in the upper crust is indicated as a fundamental mass-transfer process responsible for the compositional differentiation of Earth's crust (Brown et al., 2011; Sawyer et al., 2011). It is commonly envisaged that melts may preferentially enrich in most incompatible elements and transport them in the upper crust, thereby leaving a residual, depleted lower crust. Nevertheless, an opposite effect was observed in several leucosomes and granitic bodies showing lower concentrations of incompatible trace elements (i.e., U, Th, Y, Zr and REEs; rare earth elements) with respect to their residual source (e.g., Sawyer, 1991; Wolfram et al., 2017). It was also shown that fluid-absent partial melting is not associated with a depletion of U and Th (i.e., heat-producing elements) concentrations in residual metapelitic-derived granulite facies rocks; elevated U–Th contents are rather retained by basement terranes (Alessio et al., 2018). Lower-than-expected concentrations of trace elements in melts relative to their source were related to processes occurring during early stages of melt migration close to the source region (e.g., Sawyer, 1991). In particular, a strong control was imputed to accessory minerals (e.g., zircon, monazite and apatite) that are able to a incorporate large amount of Zr, U, Th, Y and REEs (e.g., Bea, 1996). In a recent study about the anatectic turbidites exposed on Kangaroo Island, Schwindinger et al. (2020) showed that accessory minerals such as apatite, monazite, xenotime and zircon become preferentially concentrated in the melanosomes. The authors proposed that local melt–host reaction leads to crystallization of magma oversaturated in accessory minerals close to the source region in the melanosome, away from the melt channel, thereby removing U, Th and REEs from the migrating melt. Mechanisms responsible for mass transfer and distribution of most incompatible elements, in particular U, Th, Zr, Y and REEs, during anatexis at the source area and through the crust remain open to debate.

Recent studies demonstrated that melt–rock interactions and reactive porous flow are key processes in the evolution of crustal rocks. For instance, they are responsible for the redistribution of major and trace elements in the oceanic lithosphere, leading interstitial melt, migrating through a crystal framework, to change towards more evolved compositions and trace-element enrichments (e.g., Lissenberg et al., 2013; Sanfilippo et al., 2020). Reactive porous melt flow was indicated as a process able to produce the hornblende-rich rocks (i.e., hornblendites) that commonly occur within the deep crust of magmatic arc environment (Meek et al., 2019). The proposed process involves a deformation-assisted migration and reaction of a hydrous melt through lower crustal gabbroic gneiss and is responsible for the dissolution of pre-existing anhydrous minerals and their replacement via nucleation of hydrous minerals. Pervasive melt–rock interaction involving growth of amphibole during porous flow of a hydrous silicate melt through the lower arc crust was also indicated as a viable mechanism influencing re-distribution of REEs; the growth in modified rocks of amphibole with igneous-like REE signature was specifically identified as a powerful indicator of melt–rock interaction during melt flux (Stuart et al., 2018). It is also noteworthy that hornblende fractionation in migmatites was indicated to exert a strong control on the budget of REEs during fluid-present melting of calc–alkaline arc rocks, contributing to the origin of leucogranitic magmas having high chondrite-normalized La/Yb and Sr/Y ratios typical of adakites (Reichardt and Weinberg, 2012).

This paper aims to achieve information on the effects triggered by the reactive migration of migmatite-related melts into associated mafic rocks and its role in the distribution of major and trace elements from the source region. For this purpose, I considered a portion of the Variscan lower–intermediate crust exposed in the Palmi area (southwestern Calabria, Italy) consisting of migmatitic paragneiss showing a peak metamorphic assemblage of biotite, K-feldspar, garnet, sillimanite and cordierite. I focused on amphibolites occurring as foliated, decimeter-thick layers within migmatites and as a decametric main body adjacent to paragneiss. In this contribution, I report major and trace-element composition of major minerals (amphibole, plagioclase, garnet) combined with major- and trace-element compositions of whole rocks. The data are used to assess that reactive migmatite-related melt imparted a mineralogical and geochemical signature by migrating within associated mafic rocks, where it promoted the crystallization of amphibole and accessory phases (i.e., allanite), which played an important role in the re-distribution of REEs and most incompatible elements out of the anatectic zone.

2 Geological framework and field relations

The Calabria–Peloritani terrane is a nappe-structured belt, built up during Alpine tectogenesis and located between the NW–SE-trending southern Apennines and E–W-trending Maghrebides (Amodio-Morelli et al., 1976). The terrane drifted to the present position during the Apennine orogeny and the opening of the western Mediterranean basins (Alvarez et al., 1974). The nappe-structured edifice, from top to bottom, consists of (i) Paleozoic continental-crust units with metamorphic and igneous rocks pertaining to the southern European Variscan belt (Fig. 1), (ii) Mesozoic oceanic-crust units locally affected by Alpine high-pressure/low-temperature (HP/LT) metamorphism, and (iii) carbonate rocks of the Apennine units (Bonardi et al., 2001, and references therein).

Late-Variscan continental-crust sections, tilted and nearly completely preserved, are exposed in the Sila (Dubois, 1971; Graessner and Schenk, 2001) and Serre massifs (Schenk, 1980). They are characterized by widespread low-pressure/high-temperature (LP/HT) metamorphism, intense

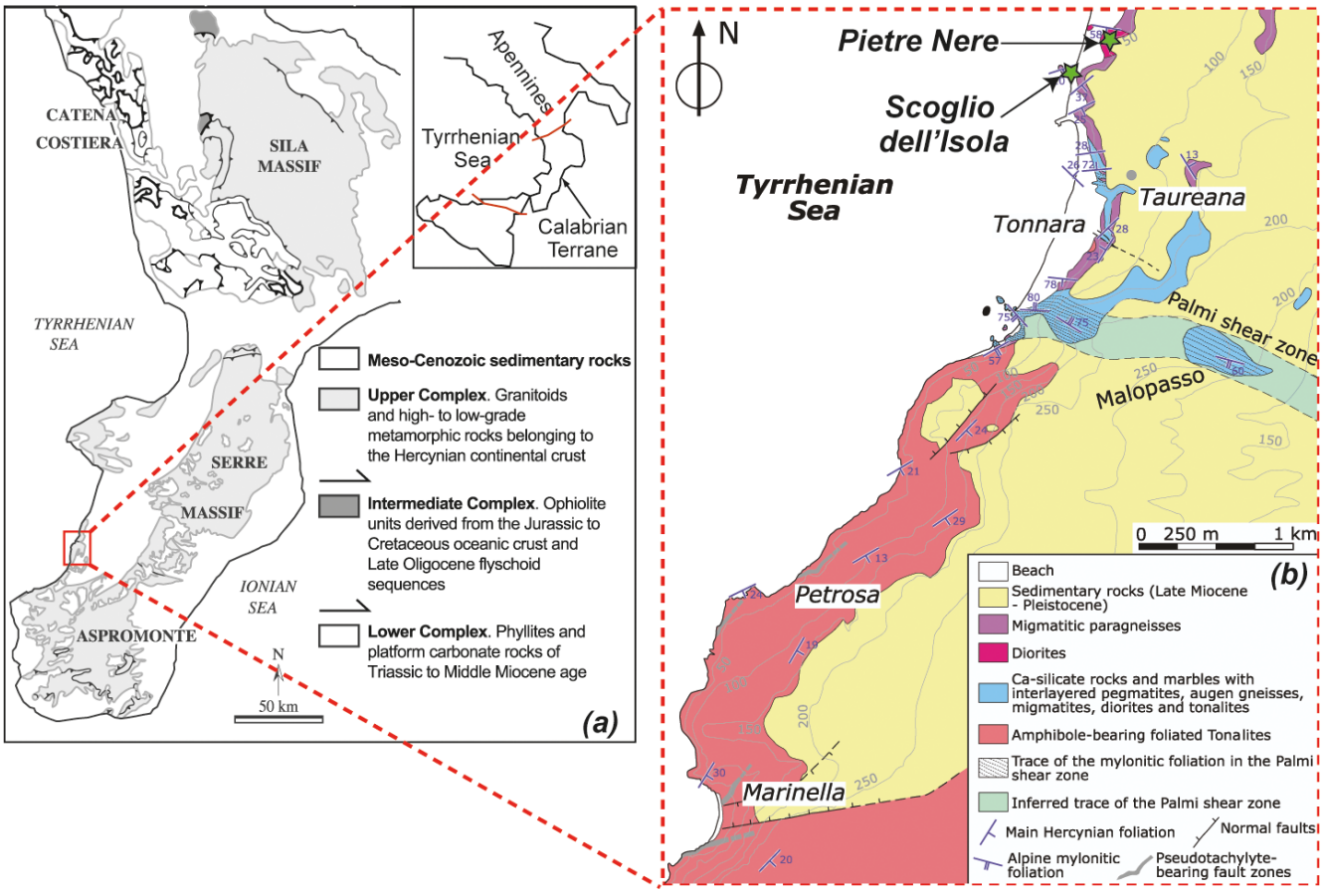

Figure 1. **(a)** Geological sketch map of Calabria, slightly modified after Festa et al. (2015), and **(b)** geological sketch map of the Palmi area, slightly modified after Caggianelli et al. (2012), and location of selected samples (green star) at Pietre Nere and Scoglio dell'Isola.

crustal anatexis and granitoid magmatism, as commonly found in other segments of the southern European Hercynian belt (e.g., Pin and Vielzeuf, 1983). In the Calabria crustal sections, granulite facies gneisses of the lower crust are overlain by tabular late-Variscan granitoids and minor gabbroic bodies emplaced at intermediate to upper-crustal levels between 306 and 290 Ma (^{40}Ar–^{39}Ar on hornblende; Ayuso et al., 1994; U–Pb on monazite; Graessner et al., 2000; U–Pb on zircon, Langone et al., 2014). The contact between granitoids and high-grade metamorphic rocks is characterized by a migmatitic border zone (Rottura et al., 1990). The granitoids intruded into overlying amphibolite and in greenschist facies metamorphic rocks of the intermediate–upper crust. Granitoids mainly consist of metaluminous calc–alkaline tonalites and granodiorites and are interpreted to originate from mantle-derived magmas hybridized by either assimilation of crustal material or mixing with crustal melts (e.g., Ayuso et al., 1994). Nearly coeval, subordinate peraluminous granites also developed by lower-crust anatexis (e.g., Rottura et al., 1993; Caggianelli et al., 2003; Fiannaca et al., 2019). Minor mafic intrusions (gabbros to diorites) of tholeiitic affinity crystallized at intermediate-crustal levels (Caggianelli et al., 1994) almost simultaneously with the intrusion of the late-Variscan granitoids. Typically, these mafic intrusions can be observed in the migmatitic border zone, as relatively small bodies on the order of some tens of meters thick (Rottura, 1985; Caggianelli and Di Florio, 1989). Moreover, they occur within tonalite and quartz-diorite as syn-plutonic dikes and enclaves (Rottura et al., 1990). The late-Variscan magmatic activity in the Calabria terrane was ended by the intrusion between 295 and 277 Ma of dike swarms ranging in compositions from microgranites and microgranodiorites to minor microgabbros and microdiorites (Festa et al., 2010).

The Palmi area is located in southwestern Calabria and comprises a portion of the Variscan lower–intermediate crust, mainly consisting of migmatitic paragneisses to the north and of amphibole-bearing tonalitic gneisses to the south (Fig. 1). The overall characteristics of the Palmi Variscan basement are similar to those observed in the Serre crustal section, where the transition zone from the mid to lower crust is exposed (Schenk, 1984). The tonalitic gneisses from Palmi show a strong foliation developed mostly at the solid state as documented by widespread presence of dynamically re-

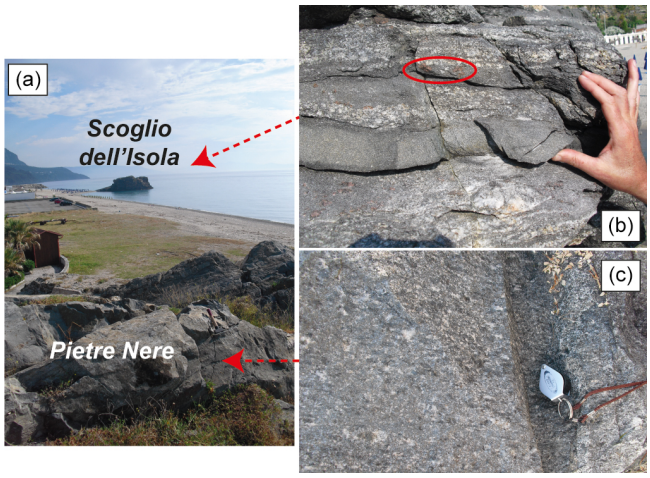

Figure 2. Photographs of **(a)** Scoglio dell'Isola and Pietre Nere outcrops, **(b)** fine-grained amphibolite layers within the migmatitic paragneiss locally containing centimeter-sized garnet grains (red circle), and **(c)** foliated domains in the Pietre Nere body.

crystallized quartz (Caggianelli et al., 1997; Prosser et al., 2003). On the basis of Al-in-hornblende geobarometer, intrusion of the tonalites within migmatitic paragneiss was estimated at 610 ± 60 MPa (Caggianelli et al., 1997). A thick marble layer is comprised between the tonalitic gneisses and migmatitic paragneiss and contain abundant clasts of calc–silicate-bearing rocks interpreted as former skarns developed during the intrusion of the tonalites. Marble acted as a weak horizon during the Eocene allowing for deformation events promoting strain localization and the production of a 400 m thick mylonitic shear zone (Prosser et al., 2003). Later deformation at the brittle–ductile transition was documented by pseudotachylyte-bearing shear zones within the tonalites and related to Oligocene extensional tectonics (Grande et al., 2009). The migmatitic paragneisses show a layering defined by the alternation of quartz–feldspar felsic bands and garnet–sillimanite–cordierite–biotite restitic layers, folded and transposed by late-Variscan high-temperature deformation (Grande et al., 2009). The paragneisses frequently include layers of calc–silicate-bearing marble, orthogneiss and metagabbro (Prosser et al., 2003).

In the Palmi area, rocks largely composed of amphibole and plagioclase (hereafter amphibolites) occur as flattened microgranular enclaves within the tonalitic gneisses (Rottura, 1985; Rottura et al., 1990) and as centimeter-thick layers or decametric bodies within the migmatitic paragneisses. Amphibolites have been studied on two main outcrops along the beach, named Scoglio dell'Isola and Pietre Nere, respectively (Figs. 1 and 2a). The former covers an area of about 1400 m^2, with a length of about 50 m towards NNW–SSE, a width of about 35 m towards ENE–WSW and a maximum elevation of about 14 m a.s.l. It is mainly composed of migmatitic paragneisses characterized by a stromatic texture with alternating melanosomes and leucosomes. The peak mineral assemblage within the melanosomes consists of biotite, K-feldspar, garnet, cordierite and sillimanite. The latter occurs as elongated prisms within the foliation or as centimeter-sized aggregates (up to 7 cm). Leucosomes are composed of quartz, feldspars (plagioclase, K-feldspars), biotite and white mica $\pm$ garnet $\pm$ cordierite. Foliated, fine-grained amphibolites occur as layers up to 10 cm thick and are locally characterized by the presence of centimetric garnet grains. Garnet is preferentially observed at the boundary between amphibolites and migmatites and is locally surrounded by a corona of biotite (Figs. 2b and 3a). Amphibolite layers are alternated with felsic ones (up to 30 cm thick) mainly composed of centimetric feldspars, quartz, biotite and garnet.

Amphibolites also occur as decametric bodies exposed on the cliff and on the beach. The outcrop on the cliff is only accessible with difficulty, whereas on the beach amphibolites occur as an isolated body (hereafter referred to as the Pietre Nere body) without exposed contacts with host rocks (Fig. 2a). The Pietre Nere body is mainly weakly to moderately foliated and fine-grained (Fig. 2c). Medium-grained, centimeter-scaled domains rarely occur; they are unfoliated and patchily associated with the fine-grained portions. Leucocratic lenses with diffuse margins characterized by relatively high plagioclase content are locally present throughout the body. On the basis of preliminary U–Pb data obtained by sector-zoned, magmatic cores of zircons separated from a Pietre Nere foliated rock, a Carboniferous age of intrusion for the parental magma was proposed (Renna et al., 2020).

3 Petrographic features of selected samples

In this study, amphibolites from the Pietre Nere body and from the layers within migmatitic paragneiss of the Scoglio dell'Isola were considered. In particular, for petrographic descriptions, whole-rock and mineral analyses, I selected (Table 1) two unfoliated medium-grained rocks (PN3 and PN4), one foliated rock (PN1) and one weakly foliated fine-grained rock (PN2) from Pietre Nere and two amphibolites interlayered with migmatitic paragneiss, which include one garnet-free (SI-1) and one garnet-bearing (SI-MR) sample.

3.1 Pietre Nere

Amphibolites from Pietre Nere mainly consist of plagioclase, amphibole and minor biotite. Medium-grained amphibolites typically show anhedral poikilitic amphibole enclosing plagioclase grains (Fig. 4a and b). Fine-grained amphibolites display an overall granoblastic texture and a foliation produced by the preferential orientation of biotite. In both medium- and fine-grained amphibolites, plagioclase (45 vol %–55 vol %) is subhedral and frequently shows 120° triple junctions (Fig. 4c). Amphibole occurs in a variable modal amount; in particular medium-grained amphibo-

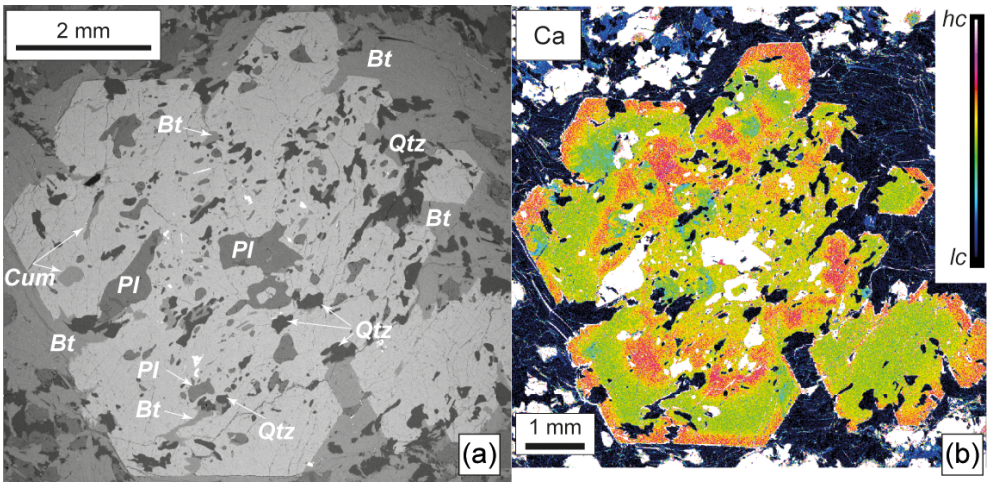

Figure 3. (a) Backscattered electron image showing the poikilitic garnet of sample SI-MR; **(b)** X-ray mapping image of the poikilitic garnet (hc: high concentration, lc: low concentration).

Table 1. Modal composition (vol %) obtained by visual estimates.

Sample	PN4 Medium-grained amphibolite	PN3 Medium-grained amphibolite	PN2 Fine-grained amphibolite	PN1 Fine-grained amphibolite	SI-1 Qtz amphibolite	SI-MR Grt amphibolite
Locality	Pietre Nere	Pietre Nere	Pietre Nere	Pietre Nere	Scoglio dell'Isola	Scoglio dell'Isola
Pl	55	45	55	52	43	40
Qtz	–	–	–	–	7	7
Cum	20	25	25	26	15	18
Hbl	25	25	15	14	10	–
Bt	tr	tr	5	8	25	30
Fe–Ti oxides	tr	5	tr	tr	tr	tr
Grt	–	–	–	–	–	5
Zrn	tr	tr	tr	tr	tr	tr
Ap	tr	tr	tr	tr	tr	tr
Aln	–	–	–	tr	tr	tr

tr < 4 %. Qtz amphibolite: quartz amphibolite. Grt amphibolite: quartz–garnet amphibolite. Extent of plagioclase alteration into fine-grained aggregates of epidote ± chlorite is ≤ 20 %. Mineral abbreviations are after Whitney and Evans (2010).

lites have slightly higher modal amount of amphibole than fine-grained amphibolites (45 vol %–50 mol % vs. 40 mol %). Poikilitic amphibole from the medium-grained amphibolites is locally composed of polygonal grains with nearly equant morphology. In fine-grained amphibolites, amphibole typically displays polygonal equant morphology (Fig. 4d); anhedral grains interstitial to plagioclase also occur. Amphibole from all Pietre Nere amphibolites is zoned with pale-brown cores and green rims (Fig. 4e), which are frequently in optical continuity. Green amphibole decreases from the modal amount of 25 vol % of the medium-grained amphibolites to the ∼ 15 vol % of the fine-grained samples (Table 1). Biotite overall occurs as subhedral grains, usually in association with amphibole, and is more abundant in fine-grained than in medium-grained amphibolites. In medium-grained amphibolites, biotite locally shows kink bands of the cleavage. Minor Fe–Ti oxides (up to 5 vol %) appear interstitial to plagioclase and amphibole; in medium-grained samples they were also found as inclusions or along the cleavage planes of green amphibole. Zircon and apatite are accessory phases. Accessory allanite associated with biotite and amphibole was also found in foliated fine-grained amphibolite (PN1, Fig. 4f).

3.2 Scoglio dell'Isola

Amphibolites interlayered with paragneiss are fine-grained and show a foliation defined by the parallel alignment of biotite and amphibole. They mainly consist of subhedral to anhedral plagioclase (40 vol %–43 vol %), variable modal abundances of anhedral amphibole (18 vol %–25 vol %) and subhedral biotite (25 vol %–30 vol %), and minor amounts of anhedral quartz (7 vol). One sample is characterized by the oc-

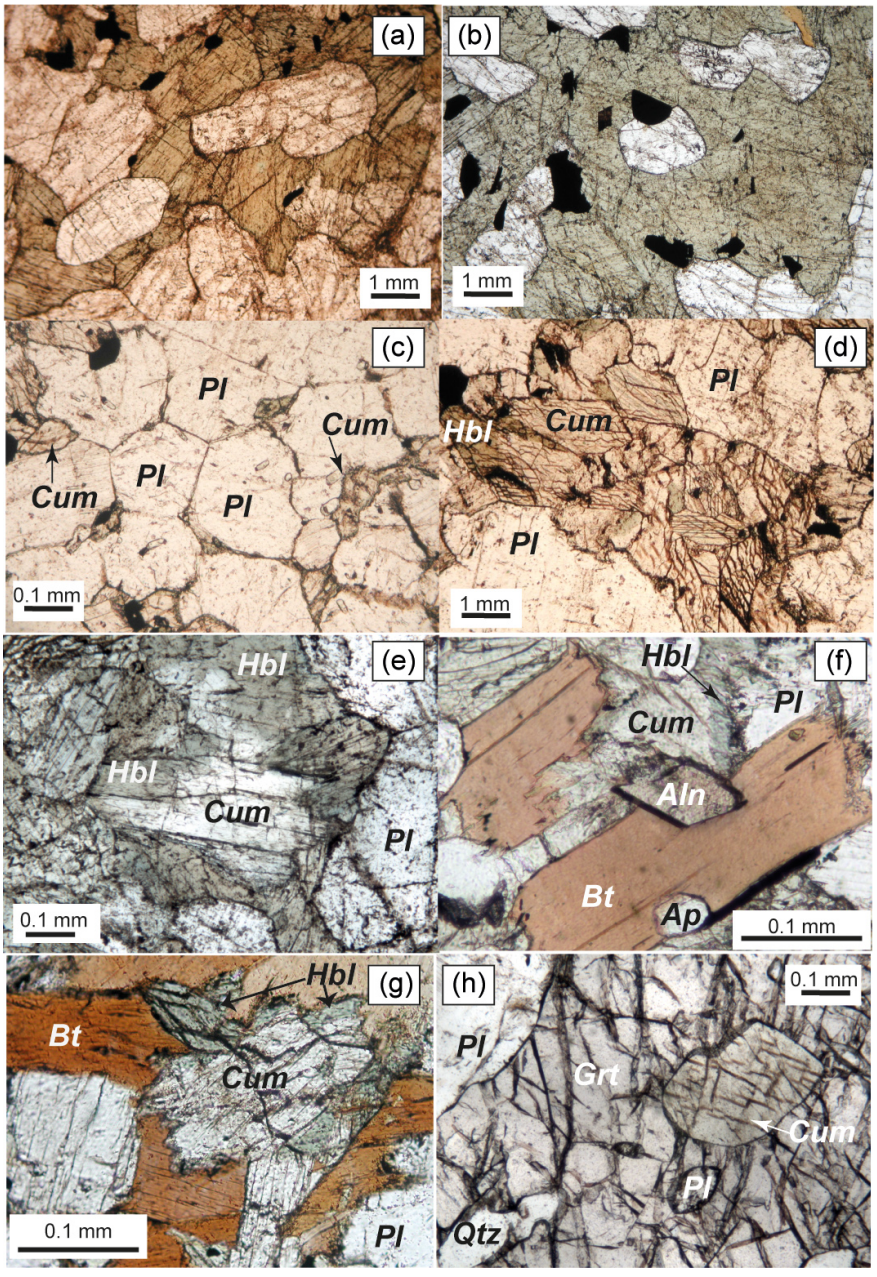

Figure 4. Thin-section photomicrographs of **(a, b)** poikilitic amphibole enclosing plagioclase grains (samples PN4 and PN3, respectively); **(c)** plagioclase showing 120° triple junctions (sample PN4); **(d)** aggregate of polygonal amphibole grains (sample PN2); **(e)** amphibole showing pale-brown (cummingtonite) core and green (hornblende) rim (sample PN4); **(f)** allanite associated with biotite and amphibole (sample PN1); **(g)** amphibole showing pale-brown (cummingtonite) core and green (hornblende) rim (sample SI-1); and **(h)** inclusions of plagioclase, quartz and cummingtonite in garnet (sample SI-MR).

currence of a centimetric garnet grain (Fig. 3). Accessory phases are Fe–Ti oxides, zircon, apatite and allanite, which commonly occur in association with biotite and amphibole.

In the garnet-free quartz amphibolite (hereafter referred to as quartz amphibolite), plagioclase locally intersects other plagioclase grains or amphibole at 120° triple junctions and amphibole is optically zoned with pale-brown cores and thin green rims (Fig. 4g). In the quartz–garnet amphibolite (hereafter referred to as garnet amphibolite), amphibole is pale brown. In this sample, garnet occurs as a poikiloblast of ~ 1 cm in size, with euhedral faces and cuspate terminations. It is mantled by biotite and minor quartz and contains numerous inclusions of plagioclase, commonly showing embayed boundaries and mainly distributed in the core.

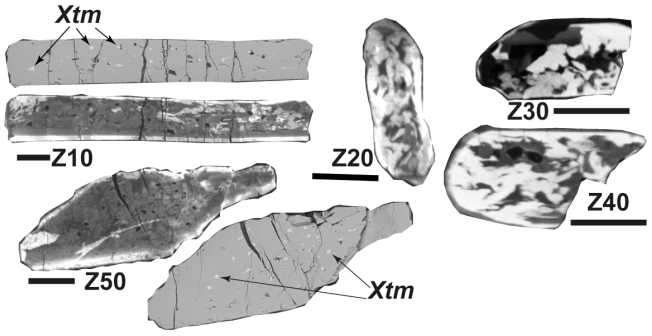

Figure 5. Cathodoluminescence images of representative zircon structures in garnet amphibolite interlayered with paragneiss and backscattered electron images of zircons Z10 and Z50, showing inclusions of xenotime (Xtm). Scale bars are 50 µm.

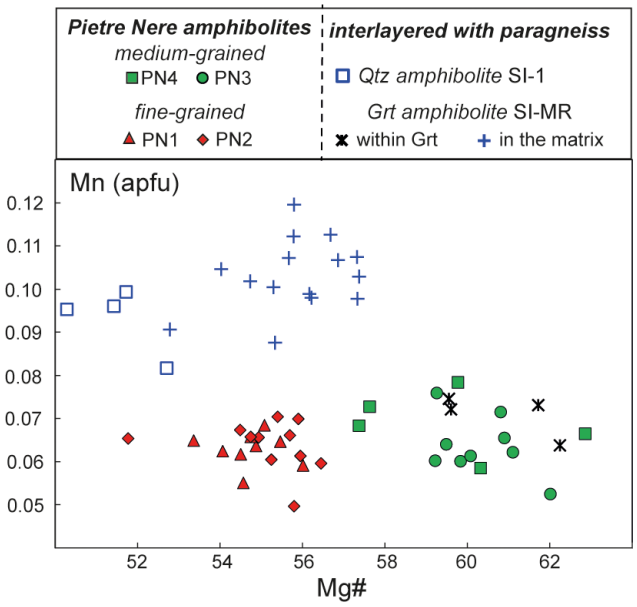

Figure 6. Variation of Mn (apfu, atoms per formula unit) vs. Mg# in cummingtonite.

Other inclusions comprise pale-brown amphibole with elliptical morphology, irregularly shaped to subhedral biotite, anhedral quartz and Fe–Ti oxides (Figs. 3 and 4h). Only one small inclusion of green amphibole was found within the garnet. Zircons from the garnet amphibolite are 50–500 µm in size and have euhedral to subhedral morphology. The internal structure of zircons from the garnet amphibolite was investigated with backscattered electron (BSE) microscopy and cathodoluminescence (CL) using a Philips XL30 electron microscope equipped with a Centaurus CL detector. Prior to the CL imaging, the sample was carbon coated and the images were obtained using 15 kV acceleration voltage and a working distance of 26 mm. CL and BSE images revealed internal structures commonly characterized by an irregularly curved patchy pattern and convolute zoning, surrounded by thin high-luminescent rims (Fig. 5). The zircons also frequently showed fractures, pores and inclusions of xenotime.

4 Mineral chemistry

Amphibole, plagioclase, biotite and garnet were analyzed for Si, Ti, Al, Cr, Fe, Mn, Ni, Mg, Ca, Na and K (Tables 2–5 and S1–S4 in the Supplement) by electron microprobe (JEOL JXA-8200 SuperProbe) at the Dipartimento di Scienze della Terra, Università degli Studi di Milano, in wavelength-dispersive spectrometry mode. For all analyses, electron microprobe operating conditions were 15 kV accelerating voltage and 5 nA beam current, counting times were 30 s on the peaks and 10 s on the backgrounds, and natural standards were used.

Trace-element mineral compositions of amphibole, plagioclase, garnet and allanite were determined by laser ablation inductively coupled plasma mass spectrometry (LA-ICP-MS) at the CNR IGG UOS of Pavia (Consiglio Nazionale delle Ricerche Istituto di Geoscienze e Georisorse Supporting Unit of Pavia; Table S5). The instrument couples a 193 nm ArF excimer laser microprobe (GeoLas200QMicrolas) to a triple quadrupole ICP-MS system (ICP-QQQ, 8900 from Agilent). NIST SRM 610 was used as an external standard; ^{44}Ca or ^{29}Si were adopted as the internal standards, depending on the mineral composition. In each analytical run the USGS reference sample BCR2 and NIST SRM 612 were analyzed together with the unknowns for quality control.

4.1 Major elements

Plagioclase from Pietre Nere amphibolites is rich in anorthitic component ranging from 80 mol % to 86 mol %. Anorthite contents in plagioclase from the quartz amphibolite interlayered with paragneiss ranges from 86 mol % to 89 mol %. In the garnet amphibolite, plagioclase in the matrix and included in the garnet have similar anorthite contents, overall ranging from 87 mol % to 91 mol % (Tables 2 and S1).

According to the classification of Hawthorne et al. (2012), pale-brown amphiboles from all selected samples are cummingtonite and green amphiboles are hornblende. Cummingtonite from the medium-grained Pietre Nere rocks have higher Mg# ($Mg/(Mg + Fe^{2+})$ in atoms per formula unit) than that from the associated fine-grained samples (57–62 vs. 51–56; Fig. 6). In the garnet amphibolite, cummingtonite within the garnet has higher Mg# (59–61) and lower MnO ($\sim$ 0.6 wt %) than that in the matrix (53–56 and 0.6 wt %–1.0 wt %). Cummingtonite from the quartz amphibolite has low Mg# (50–53) and MnO contents similar to those of cummingtonite from the matrix of the garnet amphibolite (Table 3, Fig. 6). MnO contents in cummingtonite from Pietre

Table 2. Electron microprobe analysis of plagioclase (average values, wt %).

Sample	PN4		PN3		PN2		PN1		SI1		SI_MR		SI_MR	
Rock type	M-G amph.		M-G amph.		F-G amph.		F-G amph.		Qtz amph.		Grt amph.		Grt amph.	
Mineral	Pl		Pl		Pl		Pl		Pl		Pl in matrix		Pl in Grt	
	$n = 6$	SD	$n = 8$	SD	$n = 9$	SD	$n = 6$	SD	$n = 5$	SD	$n = 19$	SD	$n = 6$	SD
SiO_2	46.6	0.5	47.2	0.4	46.8	0.6	47.4	0.4	46.2	0.6	46.1	0.3	46.1	0.7
TiO_2	< 0.04	–	< 0.04	–	< 0.04	–	< 0.04	–	< 0.04	–	< 0.04	–	< 0.04	–
Al_2O_3	34.3	0.6	33.7	0.3	33.7	0.2	33.2	0.2	34.0	0.5	34.8	0.3	34.9	0.4
FeO	0.04	0.04	0.05	0.06	0.05	0.04	0.06	0.05	0.05	0.04	0.08	0.07	0.12	0.11
MnO	< 0.01	–	< 0.01	–	< 0.01	–	< 0.01	–	< 0.01	–	< 0.01	–	< 0.01	–
MgO	< 0.01	–	< 0.01	–	< 0.01	–	< 0.01	–	< 0.01	–	< 0.01	–	< 0.01	–
CaO	18.2	0.2	16.9	0.3	17.0	0.2	16.6	0.3	17.7	0.3	18.1	0.2	18.1	0.6
Na_2O	1.66	0.16	1.87	0.21	1.78	0.12	1.98	0.22	1.38	0.16	1.29	0.12	1.29	0.34
K_2O	0.03	0.05	0.02	0.01	0.02	0.01	0.02	0.01	0.03	0.01	0.01	0.01	0.01	0.02
Sum	100.9	0.7	99.7	0.6	99.3	0.5	99.4	0.2	99.5	0.4	100.4	0.3	100.6	0.2
An (mol %)	85.7	1.4	83.2	1.8	83.9	1.0	82.2	1.9	87.5	1.5	88.5	1.1	88.5	3.1

M-G amph.: medium-grained amphibolite. F-G amph.: fine-grained amphibolite. Qtz amph.: quartz amphibolite. Grt amph.: quartz–garnet amphibolite.

Table 3. Electron microprobe analysis of cummingtonite (average values, wt %).

Sample	PN4		PN3		PN2		PN1		SI1		SI-MR		SI-MR	
Rock type	M-G amph.		M-G amph.		F-G amph.		F-G amph.		Qtz amph.		Grt amph.		Grt amph.	
Mineral	Cum		Cum		Cum		Cum		Cum		Cum in matrix		Cum in Grt	
	$n = 5$	SD	$n = 9$	SD	$n = 11$	SD	$n = 9$	SD	$n = 4$	SD	$n = 15$	SD	$n = 4$	SD
SiO_2	54.9	0.7	54.8	0.6	54.1	0.3	54.3	0.3	54.2	0.9	54.3	0.4	55.0	0.2
TiO_2	0.06	0.04	0.05	0.04	0.04	0.03	0.04	0.02	0.02	0.02	0.05	0.03	0.05	0.03
Al_2O_3	0.83	0.43	0.66	0.27	0.77	0.15	0.81	0.24	0.86	0.30	1.07	0.44	1.02	0.30
Cr_2O_3	0.01	0.01	0.01	0.01	0.02	0.02	0.02	0.04	0.01	0.01	0.01	0.01	0.01	0.02
FeO	21.9	0.6	22.5	0.6	24.9	0.6	24.9	0.3	26.0	0.3	24.7	0.5	22.4	0.5
MnO	0.56	0.06	0.52	0.06	0.51	0.05	0.51	0.03	0.75	0.07	0.84	0.07	0.59	0.04
MgO	18.0	1.4	18.8	0.4	17.1	0.4	16.9	0.4	15.5	0.5	17.1	0.5	19.1	0.5
CaO	0.91	0.30	0.78	0.25	0.68	0.11	0.73	0.16	0.73	0.23	1.11	0.35	0.86	0.33
Na_2O	0.05	0.05	0.03	0.02	0.05	0.02	0.07	0.02	0.07	0.04	0.10	0.06	0.10	0.03
K_2O	0.01	0.01	0.02	0.01	0.01	0.01	0.02	0.01	0.02	0.03	0.01	0.01	0.00	0.01
Sum	97.2	1.6	98.2	0.5	98.2	0.4	98.3	0.4	98.2	0.6	99.3	0.3	99.1	0.4
Mg#	59.6	2.2	60.3	1.0	55.1	1.3	54.7	0.8	51.5	1.0	55.8	1.3	60.8	1.4

M-G amph.: medium-grained amphibolite. F-G amph.: fine-grained amphibolite. Qtz amph.: quartz amphibolite. Grt amph.: quartz–garnet amphibolite. $Mg\# = 100 \times Mg^{2+}/(Mg^{2+} + Fe^{2+})$.

Nere rocks are relatively low (0.4 wt %–0.6 wt %). Estimated Fe ratios ($Fe^{2+}/(Fe^{2+} + Fe^{3+}$) overall range from 0.94 to 1.00 with an average of 0.99 (Table S2). The cummingtonite has 0.4 wt %–1.7 wt % of Al_2O_3 and 0.5 wt %–1.7 wt % of CaO.

Mg# of hornblende from the medium-grained Pietre Nere amphibolites is higher than that from fine-grained samples (62–67 vs. 44–54; Fig. 7). In Pietre Nere rocks, hornblende has also variable contents of Al_2O_3 (7.0 wt %–18.0 wt %) and CaO (7.0 wt %–12 wt %) and low amounts of K_2O (0.2 wt %–0.4 wt %). Hornblende from the fine-grained amphibolites frequently shows higher Al_2O_3 and lower SiO_2 than that from the medium-grained samples (Fig. 7). Hornblende from the quartz amphibolite has low Mg# (39–45) and SiO_2 ($\sim$ 43 wt %) and relatively high Al_2O_3 (14 wt %–16 wt %) and K_2O (0.4 wt %–0.5 wt %). Hornblende included within garnet has relatively high Mg# and SiO_2 (60 wt % and 47 wt %) and low Al_2O_3 (11 wt %). Estimated Fe ratios ($Fe^{2+}/(Fe^{2+} + Fe^{3+})$) overall range from 0.89 to 1.00 with an average of 0.99 (Table S3). Hornblende has TiO_2 in the range of 0.1 wt % to 0.9 wt %.

Biotite from fine-grained Pietre Nere amphibolites differs from that of associated medium-grained samples for the higher $Fe^{2+}_{tot}/(Fe^{2+}_{tot} + Mg)$ values, which are in the range of 0.41–0.44 and 0.33–0.39, respectively (Tables 5 and S4). In the garnet amphibolite, biotite within the poikilitic garnet has lower $Fe^{2+}_{tot}/(Fe^{2+}_{tot} + Mg)$ values than that in the matrix (0.33–0.37 vs. 0.40–0.44). High $Fe^{2+}_{tot}/(Fe^{2+}_{tot} + Mg)$ values were found for the biotite from the quartz amphibolite (0.47–0.53). Overall, biotite has TiO_2 from 1.7 wt % to 2.8 wt % and Na_2O from 0.1 wt % to 0.4 wt %. Biotite from the garnet amphibolite is characterized by high K_2O (9.0 wt %–10.0 wt %), which frequently exceed those of biotite from other samples (8.2 wt %–9.2 wt %).

Garnet is almandine-rich (Alm_{60-69}, Gr_{7-14}, Py_{13-19}, Sps_{7-9}) and shows (i) a rough, oscillatory zoning for Ca, which is higher along the garnet rim and in the core, slightly

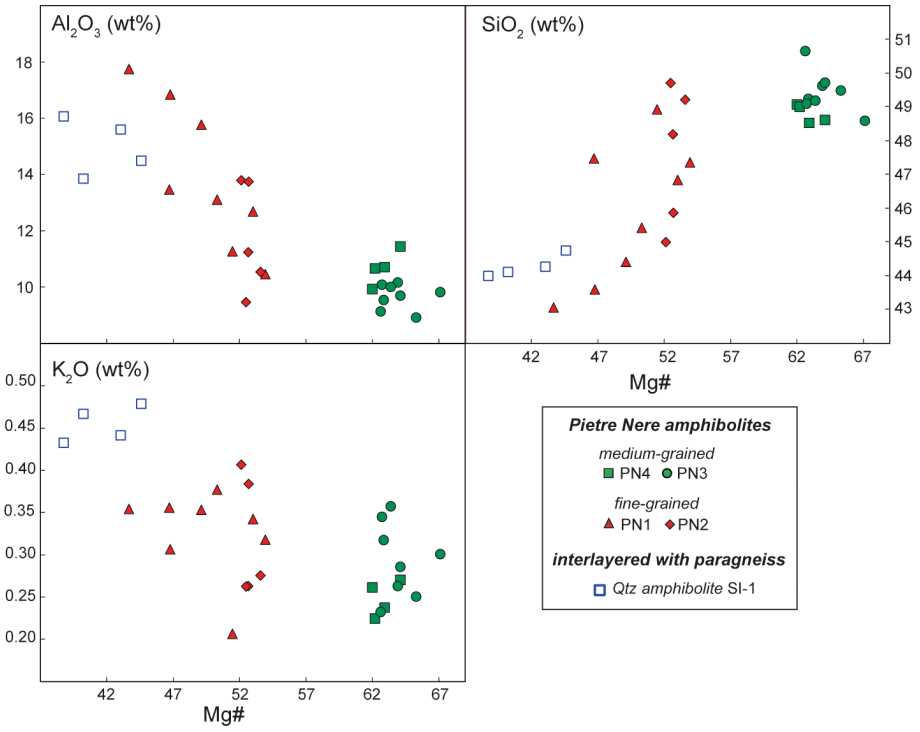

Figure 7. Variation of Al_2O_3 (wt %), SiO_2 (wt %) and K_2O (wt %) vs. Mg# in hornblende.

Table 4. Electron microprobe analysis of hornblende (average values, wt %).

Sample	PN4		PN3		PN2		PN1		SI1		SI-MR
Rock type	M-G amph.		M-G amph.		F-G amph.		F-G amph.		Qtz amph.		Grt amph.
Mineral	Hbl		Hbl		Hbl		Hbl		Hbl		Hbl in garnet
	$n = 4$	SD	$n = 6$	SD	$n = 5$	SD	$n = 8$	SD	$n = 4$	SD	$n = 1$
SiO_2	47.1	0.2	47.7	0.6	46.0	1.9	44.5	1.9	43.0	0.3	47.0
TiO_2	0.77	0.07	0.73	0.18	0.57	0.14	0.48	0.23	0.40	0.27	0.67
Al_2O_3	10.7	0.6	9.61	0.51	11.8	1.9	13.91	2.62	15.0	1.0	10.7
Cr_2O_3	0.03	0.02	0.02	0.02	0.04	0.03	0.07	0.05	0.06	0.05	0.08
FeO	13.6	0.5	14.0	0.9	17.6	1.4	17.0	0.8	18.8	1.0	14.3
MnO	0.17	0.04	0.19	0.03	0.23	0.07	0.20	0.05	0.26	0.02	0.12
MgO	12.7	0.02	13.6	0.6	11.0	1.0	9.36	1.5	7.52	0.59	12.1
CaO	11.8	0.3	10.5	1.1	9.14	1.78	10.5	1.2	11.3	0.3	11.6
Na_2O	0.96	0.08	0.87	0.09	1.01	0.20	1.17	0.19	1.11	0.13	1.02
K_2O	0.25	0.02	0.28	0.04	0.32	0.07	0.33	0.05	0.45	0.02	0.37
Sum	98.1	0.5	97.5	0.6	97.7	0.5	97.5	0.5	97.9	0.5	97.9
Mg#	62.8	1.0	64.1	1.8	52.7	0.5	49.4	3.5	41.7	2.6	60.1

M-G amph.: medium-grained amphibolite. F-G amph.: fine-grained amphibolite. Qtz amph.: quartz amphibolite. Grt amph.: quartz–garnet amphibolite.
$Mg\# = 100 \times Mg^{2+}/(Mg^{2+} + Fe^{2+})$.

Table 5. Electron microprobe analysis of biotite (average values, wt %).

Sample	PN3		PN2		PN1		SI1		SI-MR		SI-MR	
Rock type	M-G amph.		F-G amph.		F-G amph.		F-G amph.		Grt amph.		Grt amph.	
Mineral	Bt		Bt		Bt		Bt		Bt in matrix		Bt in Grt	
	$n = 6$	SD	$n = 3$	SD	$n = 3$	SD	$n = 3$	SD	$n = 10$	SD	$n = 6$	SD
SiO_2	38.1	0.1	37.3	0.3	37.9	0.4	36.8	0.3	37.7	0.2	38.3	0.3
TiO_2	2.29	0.20	1.94	0.24	2.13	0.21	2.58	0.36	2.52	0.21	2.31	0.28
Al_2O_3	17.3	0.4	17.6	0.2	17.2	0.3	16.8	0.6	16.7	0.4	16.5	0.4
Cr_2O_3	0.02	0.02	0.07	0.07	0.04	0.03	0.06	0.05	0.04	0.02	0.03	0.04
FeO	14.8	0.8	17.1	0.4	17.2	0.2	19.1	1.4	17.2	0.6	14.9	0.6
MnO	0.04	0.03	0.05	0.03	0.03	0.04	0.07	0.03	0.06	0.02	0.04	0.02
MgO	14.7	0.6	12.9	0.5	12.6	0.2	10.8	0.7	13.2	0.2	15.3	0.5
CaO	0.09	0.09	0.04	0.03	0.02	0.02	0.04	0.02	0.02	0.01	0.05	0.03
Na_2O	0.12	0.07	0.14	0.04	0.24	0.04	0.19	0.02	0.18	0.04	0.32	0.13
K_2O	8.70	0.28	8.50	0.33	8.66	0.12	8.87	0.28	9.70	0.14	9.15	0.43
Sum	96.2	0.6	95.6	0.7	96.0	0.6	95.3	1.0	97.3	0.4	96.9	0.5
Fe#	36.2	2.1	42.7	1.4	43.5	0.2	49.7	3.3	42.2	1.1	35.5	1.5

M-G amph.: medium-grained amphibolite. F-G amph.: fine-grained amphibolite. Qtz amph.: quartz amphibolite. Grt amph.: quartz–garnet amphibolite. $Fe\# = 100 \times Fe^{2+}/(Fe^{2+} + Mg)$.

decreasing in the intermediate zone, and (ii) slight depletion of Mg towards the rims (Fig. 3, Tables 6 and S4).

4.2 Trace-element compositions

4.2.1 Amphibole and plagioclase

The chondrite-normalized REE pattern of cummingtonite from Pietre Nere amphibolites shows negative Eu anomaly ($Eu / Eu^* \sim 0.6$) and LREE (light rare earth element) depletion with respect to MREEs (middle rare earth elements) and HREEs (heavy rare earth elements), which are nearly flat at ~ 10 times chondrite (Fig. 8). Cummingtonite from the fine-grained amphibolite PN1 differs for a more marked LREE depletion ($Ce_N / Sm_N = 0.2$ for $Sm_N = 12$) with respect to other Pietre Nere samples ($Ce_N / Sm_N = 0.6$ for $Sm_N = 13$). Within each sample, the REE pattern of hornblende is parallel to that of the associated cummingtonite. The hornblende has higher absolute REE concentrations (by about an order of magnitude) with a pattern exhibiting a slight decrease from Gd to Lu ($Gd_N / Lu_N = 2.0$–2.7 for $Lu_N = 35$–58) and a marked negative Eu anomaly ($Eu / Eu^* = 0.4$). With respect to cummingtonite, hornblende is also characterized by higher V, Cr and Sc concentrations (Table S5). Overall, both hornblende and cummingtonite from the fine-grained sample PN1 have higher V, Cr and Sc than those from other Pietre Nere amphibolites.

Cummingtonite and hornblende from Pietre Nere amphibolites have parallel chondrite-normalized incompatible-element patterns, which overall show Rb, Ba, Nb and Ta depletion with respect to MREEs–HREEs and Y; Sr depletion relative to Ce–Nd by about 2 orders of magnitude; and Zr, Hf and Ti depletion relative to MREEs and HREEs by about 1 order of magnitude (Fig. 8). Incompatible-trace-element contents are higher by about an order of magnitude in hornblende than in cummingtonite. Both cummingtonite and hornblende from fine-grained amphibolite PN1 are enriched in Rb and Ba with respect to those from other Pietre Nere rocks.

Cummingtonite from the quartz amphibolite and from the matrix of the garnet amphibolite have roughly parallel chondrite-normalized REE patterns characterized by a prominent depletion of LREEs relative to MREEs ($Ce_N / Sm_N = 0.02$–0.05 for $Sm_N = 31$–6) and an increase from Gd to Lu ($Gd_N / Lu_N = 0.2$–0.7 for $Lu_N = 108$–76). Cummingtonite from the garnet amphibolite differs for a less marked negative Eu anomaly ($Eu / Eu^* = 0.5$ vs. 0.1) and lower concentrations of LREEs and MREEs, which most likely reflect simultaneous crystallization with an LREE-rich phase (i.e., allanite; see Figs. 8 and 9). In the garnet amphibolite, cummingtonite within garnet is distinct in showing a decrease from Gd to Lu ($Gd_N / Lu_N = 2.2$ for $Lu_N = 9$). Hornblende from the quartz amphibolite has a parallel chondrite-normalized REE pattern to associated cummingtonite but at higher concentration levels (by about an order of magnitude) and with a decrease from Gd to Lu ($Gd_N / Lu_N = 2.1$ for $Lu_N = 620$). V, Cr and Sc are significantly higher in hornblende relative to cummingtonite (Table S5). The chondrite-normalized incompatible-element patterns of cummingtonite overall show Rb, Ba, Nb, Ta, Sr and HFSE (high-field-strength element) (Nb, Ta, Zr, Hf and Ti) depletion with respect to MREEs–HREEs and Y (Fig. 8). Rb, Ba, Nb and Ta are also enriched relative to La–Ce. Hornblende has a parallel chondrite-normalized incompatible-element pattern to associated cummingtonite but at higher concentration levels (by about an order of magnitude).

Plagioclase from Pietre Nere amphibolites (Fig. 9) have nearly similar chondrite-normalized REE patterns, which

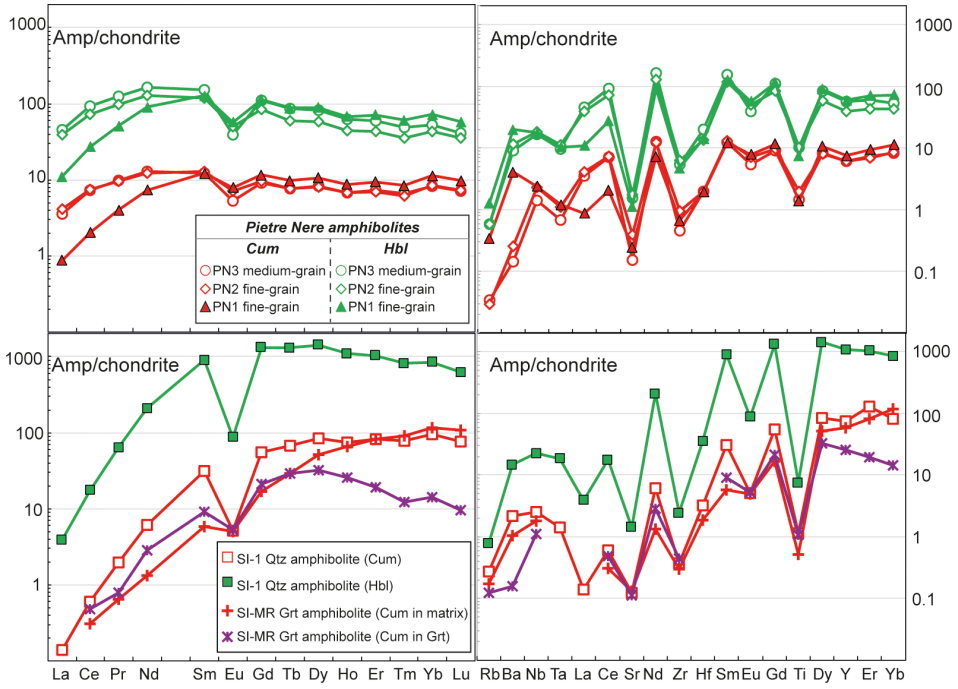

Figure 8. REE and incompatible-trace-element compositions normalized to chondrite (Anders and Ebihara, 1982) of cummingtonite and hornblende.

Table 6. Electron microprobe analysis of garnet (average values, wt %).

Sample	SI-MR		SI-MR		SI-MR	
Rock type	Grt amph.		Grt amph.		Grt amph.	
Mineral	Grt rim		Grt interim		Grt core	
	$n = 4$	SD	$n = 4$	SD	$n = 8$	SD
SiO_2	38.5	0.4	38.4	0.2	38.9	0.2
TiO_2	< 0.04	–	< 0.04	–	< 0.04	–
Al_2O_3	22.1	0.2	21.9	0.2	22.2	0.1
Cr_2O_3	0.03	0.03	0.03	0.02	0.03	0.02
FeO	29.9	0.1	31.0	0.2	28.9	0.7
MnO	3.54	0.32	3.39	0.11	3.34	0.26
MgO	3.59	0.38	4.00	0.11	4.57	0.15
CaO	5.13	0.14	4.11	0.21	5.25	0.53
Na_2O	0.02	0.03	0.02	0.03	0.02	0.02
K_2O	< 0.01	–	< 0.01	–	< 0.01	–
Sum	102.8	0.5	102.9	0.2	103.2	0.3
Prp	14.2	1.5	16.1	0.6	17.9	0.5
Alm	65.2	0.7	67.7	0.7	62.1	1.5
Grs	12.6	1.1	8.50	1.19	12.6	1.2
Sps	7.96	0.75	7.74	0.32	7.43	0.58

Grt amph.: quartz–garnet amphibolite.

display a marked LREE enrichment relative to MREEs ($La_N / Sm_N = 18–22$ for $Sm_N = 1.2–1.8$), a prominent positive Eu anomaly ($Eu / Eu^* = 27–38$) and a steady decrease from Gd to Er ($Gd_N / Er_N \sim 7$ for $Er_N \sim 0.1$). In the quartz amphibolite, the REE pattern of plagioclase is characterized by a flat LREE ($La_N / Sm_N = 1.0$ for $Sm_N = 7.0$) and a moderate positive Eu anomaly ($Eu / Eu^* = 8$) and depletion of HREEs relative to MREEs ($Gd_N / Er_N = 7$ for $Er_N = 0.5$).

4.2.2 Garnet and allanite from the garnet amphibolite

The core of the poikilitic garnet has a chondrite-normalized REE pattern (Fig. 9) showing HREE enrichment with respect to MREEs ($Gd_N / Lu_N = 0.21$ for $Lu_N = 490$) and a marked negative Eu anomaly ($Eu / Eu^* = 0.1$). Normalization to chondrite reveals that the rim of the garnet differs for a nearly flat HREE pattern, which are at lower concentration levels (by a factor of ~ 5) and a slight negative Eu anomaly ($Eu / Eu^* = 0.5$).

The chondrite-normalized REE pattern of allanite (Fig. 9) is characterized by a marked enrichment of LREE relative to MREEs ($La_N / Sm_N = 5.7$ for $Sm_N = 32\,294$), a prominent negative anomaly ($Eu / Eu^* = 0.2$) and a steady decrease from Gd to Lu ($Gd_N / Lu_N = 36$ for $Lu_N = 381$). Uranium and Th contents are high (1130 and 1750 ppm, respectively). Allanite also has relatively high contents of Ti, Ba, V, Cr and Sc (Table S5).

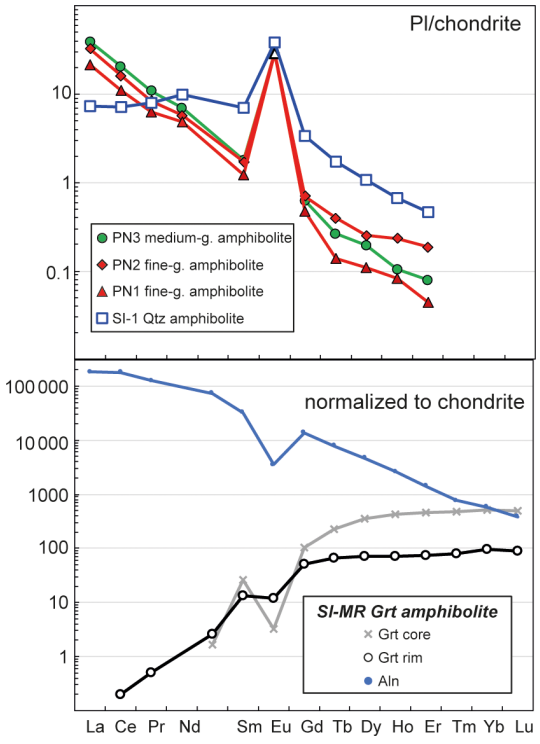

Figure 9. REE compositions normalized to chondrite (Anders and Ebihara, 1982) of plagioclase, garnet and allanite.

5 Whole-rock chemistry

Whole-rock major- and trace-element analyses of the selected rocks (Table S6) were carried out at Activation Laboratories (Ancaster, Ontario) by inductively coupled plasma (ICP) optical emission spectroscopy and ICP mass spectrometry (4Lithores method of lithium metaborate and tetraborate fusion, ICP, and ICP-MS). Three blanks and five controls (three before sample group and two after) were analyzed per group of samples. Precision and accuracy are estimated to be better than 2 % for SiO_2, Al_2O_3, Fe_2O_3 and MgO and better than 5 % for the other major elements. Precision and accuracy of trace-element analyses are typically assessed to be within 10 %.

Medium-grained amphibolites from Pietre Nere have higher Mg# (molar $Mg/(Mg + Fe^{2+}_{tot}) \times 100 = 57–59$) than associated fine-grained samples (50–51, Fig. 10). Fine-grained amphibolite PN1 has lower CaO and higher K_2O than other Pietre Nere samples, which overall range from 10.1 wt % to 11.0 wt % and from 0.41 wt % to 0.56 wt %, respectively. The TiO_2 concentrations are higher in medium-grained amphibolite PN3 than in other Pietre Nere samples, which reflects its higher modal content of Fe–Ti oxides (Table 1), as also confirmed by normative calculations revealing a significant amount of normative ilmenite in this sample (Table S6). The garnet amphibolite has higher Mg# than quartz amphibolite (54 and 49, respectively). The samples interlayered with the paragneiss are also characterized by relatively low CaO (7.0 wt %–8.7 wt %) and Na_2O (0.6 wt %–0.8 wt %) and high K_2O (2.3 wt %–4.0 wt %). Amphibolites have overall Al_2O_3 in the range of 19 wt % to 21 wt % (Fig. 10) and relatively low SiO_2 / Al_2O_3 values (2.2 to 2.5, Table S6). Medium-grained amphibolites from Pietre Nere have the highest contents of V (280–487 ppm), which reflects the higher modal content of (i) hornblende, which is characterized by high V concentrations (Table S5), and (ii) Fe–Ti oxides for which V is a compatible element (Best, 2003). The concentrations of Ni and Cr are overall low (< 30 ppm and 30–100 ppm, respectively).

The chondrite-normalized REE patterns (Fig. 11) of fine-grained amphibolites and medium-grained amphibolite PN4 from Pietre Nere are characterized by LREE enrichment over HREEs ($La_N / Yb_N = 4.2–10.5$ for $Yb_N = 5.7–8.4$). The REE pattern of these samples also displays a positive Eu anomaly ($Eu / Eu^* = 1.5–1.8$). Fine-grained samples are slightly LREE enriched and HREE depleted relative to sample PN4. The REE pattern of medium-grained amphibolite PN3 differs from those of other Pietre Nere rocks for showing slightly higher MREE and HREE contents (by a factor of ~ 2), a slight depletion of LREEs relative to MREEs and negative Eu anomaly ($Eu / Eu^* = 0.6$), which may be related to a relatively high modal amphibole / plagioclase ratio (Table 1). The chondrite-normalized REE pattern of the

garnet amphibolite shows a steady decrease from LREEs to HREEs ($La_N / Yb_N = 8.1$ for $Yb_N = 15$) and a weak positive Eu anomaly ($Eu / Eu^* = 1.1$). The quartz amphibolite displays LREE depletion relative to MREEs, which are in turn enriched over HREEs ($Gd_N / Yb_N = 1.7$ for $Yb_N = 26$), and a negative Eu anomaly ($Eu / Eu^* = 0.5$). It is noteworthy that REE patterns of the quartz and garnet amphibolites are approximately parallel to those of medium-grained sample PN3 and fine-grained rocks from Pietre Nere, respectively, but at slightly higher concentration levels.

In the chondrite-normalized multi-element diagram, Pietre Nere amphibolites display the enrichment of Ba, Nb and Sr relative to Rb, Th, Zr and Y (Fig. 11). Fine-grained amphibolite PN1 differs from other Pietre Nere samples in showing higher contents of Rb, Ba and Th and Zr enrichment over Y. Amphibolites interlayered with the paragneiss are characterized by a significant enrichment of Rb, Ba, Th and Nb with respect to Sr, Zr and Y.

6 Discussion

6.1 The protolith of Palmi amphibolites

In the Palmi area (southwestern Calabria, Italy), a Variscan lower–intermediate crust is exposed and mainly consists of amphibole-bearing tonalitic gneisses and migmatitic paragneiss. Amphibolites occur in close spatial relationship with migmatitic paragneiss (Fig. 1). In particular, amphibolites are present as foliated, decimeter-thick layers within migmatites and as a decametric main body (i.e., Pietre Nere body) adjacent to the paragneiss (Fig. 2). The Pietre Nere body is mainly fine-grained and variably foliated, even though unfoliated, medium-grained portions rarely occur. Amphibolites from the Pietre Nere body and interlayered with paragneiss share a similar mineralogical composition mainly composed of anorthite-rich plagioclase (An_{80-91}), amphibole consisting of cummingtonite rimmed by hornblende and biotite. Amphibolite layers within paragneiss contain minor quartz, accessory allanite and locally garnet. Accessory allanite also locally occurs in foliated, fine-grained Pietre Nere amphibolites.

Based on their SiO_2 contents (47 wt %–49 wt %, calculated water free), all amphibolites have a basic composition and fall in the basaltic (gabbroic) field of the total alkali vs. silica diagram (TAS, Best, 2003; Fig. S1 in the Supplement). All samples are characterized by high amount of normative anorthite and hypersthene (Table S6). Furthermore, one sample from the Pietre Nere body and one interlayered with paragneiss are slightly olivine normative, thereby indicating that amphibolites likely derived from a mafic igneous protolith. Relic of texture that may be reconciled with a magmatic origin is represented by the poikilitic morphology of amphibole in unfoliated, medium-grained rocks from Pietre Nere (Fig. 4a and b). The above analogy in terms of modal, normative and whole-rock major-element compositions and the fact that amphibolites interlayered with paragneiss have approximately parallel REE patterns to amphibolites from Pietre Nere (Fig. 11) suggest a genetic relationship among these rocks. Furthermore, whole-rock compositions suggest that the protolith of amphibolites had a cumulus origin, in particular the low SiO_2 / Al_2O_3 values (Table S6), and the frequent occurrence of positive Eu anomaly in REE patterns

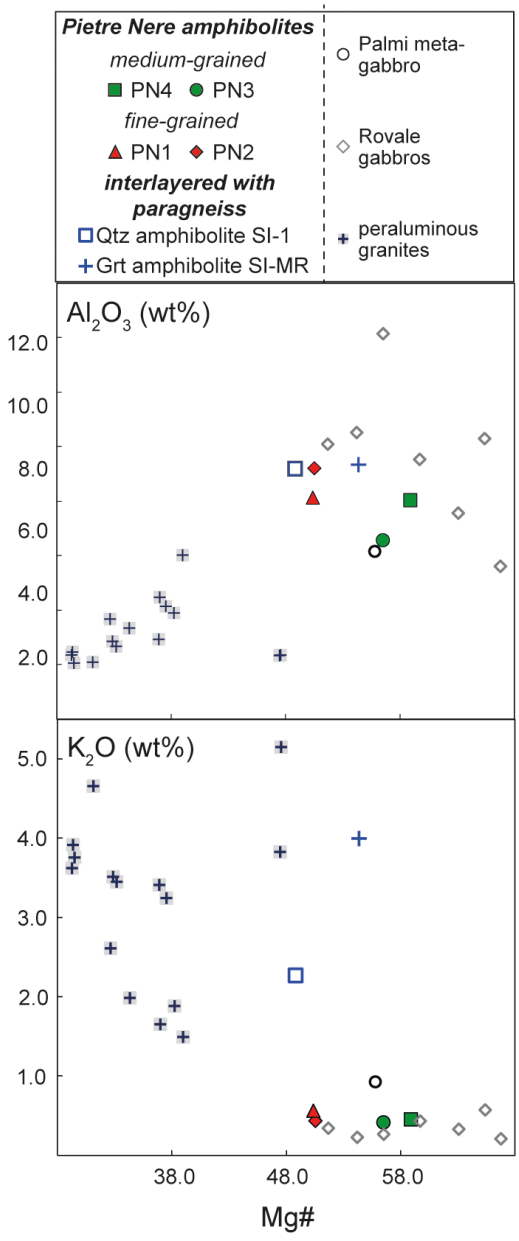

Figure 10. Major-element whole-rock variation (calculated water free): Al_2O_3 (wt %) and K_2O (wt %) vs. Mg#. The compositions of metagabbro associated with Palmi tonalitic gneisses (Rottura, 1985) of Rovale gabbros (Sila Massif, Caggianelli et al., 1994) and late-Variscan peraluminous granites (central and southern Calabria, Rottura et al., 1993; Fiannacca et al., 2019) are reported for comparison.

(Fig. 11) provide evidence for a plagioclase-bearing cumulate nature for these rocks (see Kempton and Harmon, 1992). The relatively low Mg# values (49 to 59) and low concentrations of Ni and Cr (Table S6) suggest a formation by melts that had previously undergone fractional crystallization.

The late-Variscan mafic intrusion of Rovale (Sila Massif, northern Calabria) includes olivine-bearing cumulates ranging from norites to amphibole–gabbros, emplaced at mid-crustal level ($P \sim 4$ kbar, pressure, Caggianelli et al., 1994). They formed by early precipitation of plagioclase and olivine and late crystallization of orthopyroxene, amphibole and biotite. Olivine has a low forsterite component (63 mol %–68 mol %), and orthopyroxene is characterized by Mg# ranging from 71 to 75. Amphibole, essentially Ti-pargasite, occurs as poikilitic grains enclosing plagioclase, which overall has 78 mol %–90 mol % of anorthite component. The Rovale gabbroic rocks have enriched Nd and Sr isotopic signatures indicating a significant crustal contribution in their origin ($\varepsilon_{\mathrm{Nd}_i} = -6.1$ and $^{87}\mathrm{Sr}/^{86}\mathrm{Sr}_i = 0.7091$–0.7095). Amphibolites from Palmi have comparable Mg# and Al_2O_3 with Rovale gabbros (Fig. 10). Palmi amphibolites and Rovale gabbros also consist of similar anorthite-rich plagioclase. In addition, Palmi amphibolites have similar chondrite-normalized REE patterns to those of gabbros from Rovale controlled by plagioclase accumulation and high amphibole modal amount (Fig. 11). The original mineralogical and geochemical composition of the protolith of Palmi amphibolites could approximately resemble that of cumulate gabbroic rocks from the Rovale mafic intrusion, thereby suggesting that the late-Variscan evolution of the Calabria terrane was characterized by mid–lower-crust intrusion of chemically comparable basic melts.

6.2 Evidence of subsolidus re-equilibration

All amphibolites provide evidence for extensive subsolidus re-equilibration at high temperature, which for instance resulted in the development of 120° triple junctions among plagioclase grains (Fig. 4c). In addition, amphibolites experienced an episode of deformation which developed heterogeneously textured rocks, namely foliated amphibolites interlayered with paragneiss; variably foliated fine-grained Pietre Nere amphibolites; and unfoliated, medium-grained Pietre Nere portions where the formation of kink bands in biotite was observed.

Assuming a pressure condition of 6.1 kbar, in agreement with the barometric estimates obtained for the emplacement of the tonalite (Caggianelli et al., 1997), the calcic-amphibole-based geothermometer of Putirka (2016) gave values of 773 to 806 °C for Pietre Nere amphibolites and of 803 °C for the quartz amphibolite interlayered with paragneiss. For the quartz amphibolite, the amphibole–plagioclase geothermometer of Holland and Blundy (1994) was also used, assuming the existence of equilibrium conditions between hornblende and plagioclase (see Sect. 6.3). The edenite–tremolite calibration of the amphibole–plagioclase geothermometer estimated a temperature of 882 °C ($T_{\mathrm{ed-tr}}$). A slightly lower temperature of 828 °C ($T_{\mathrm{ed-ri}}$) was obtained by using the edenite–richterite calibration. In the cases in which $T_{\mathrm{ed-tr}}$ is higher than $T_{\mathrm{ed-ri}}$, the latter is indicated to represent that of equilibrium (Holland and Blundy, 1994); I thus considered the temperature of 828 °C as those of crystallization of hornblende–plagioclase pairs in the quartz amphibolite. Taking into account the uncertainties of the methods, namely the accuracy of ±30 and ±40 °C for the calibration of Putirka (2016) and Holland and Blundy (1994), temperatures estimated for amphibolites from Pietre Nere and the quartz amphibolite interlayered with paragneiss are overlapping and specifically in the range of 743–836 and 788–868 °C, respectively. Overall, these temperature evaluations are consistent with a re-equilibration under granulite facies metamorphic conditions of the mafic protolith.

6.3 Origin of amphibole by reactive melt migration

Amphibole is ubiquitous in all amphibolites from the Palmi area and mostly consists of cummingtonite cores rimmed by hornblende (Fig. 4). Cummingtonite is often described in rocks formed under conditions ranging from upper greenschist to the beginning of granulite facies conditions (e.g., Mottana et al., 1994; Schumacher, 2007). The entire stability range for cummingtonite was thermodynamically constrained at 400–800 °C and < 1–15 kbar (Evans and Ghiorso, 1995). Cummingtonite was also observed as a magmatic phase in dacites and rhyolites (e.g., Geschwind and Rutherford, 1992; Deering et al., 2008). Fractional crystallization experiments conducted at 0.7 GPa for hydrous, calc–alkaline to arc-tholeiitic magmas showed that cummingtonite crystallizes at temperatures below 780 °C, coexisting with a rhyolitic liquid and a mineralogical assemblage characterized by a plagioclase with ∼ 40 mol %–65 mol % of anorthite component (Nandedkar et al., 2014, 2016). Furthermore, the thermodynamic model by Evans and Ghiorso (1995) showed that cummingtonite, when present, should be associated with relatively Na-rich plagioclase. In the Palmi amphibolites, the primary crystallization of cummingtonite in association with the anorthite-rich plagioclase is thus incompatible with experiments and natural occurrence of this amphibole in magmatic rocks of silicic compositions. The involvement of an exotic agent after the formation of early plagioclase is required to explain the crystallization of cummingtonite in the Palmi amphibolites.

In gabbros, the origin of cummingtonite is sometimes attributed to interaction between orthopyroxene and a late magmatic aqueous fluid phase (e.g., Roberts et al., 2000) or SiO_2-rich hydrous melt (e.g., Elburg, 1996). In metabasic rocks from the Serre and Sila massifs (central and northern Calabria) the origin of cummingtonite was related to hydration of granulite facies orthopyroxene, according to the following reaction (mineral abbreviations after Whitney

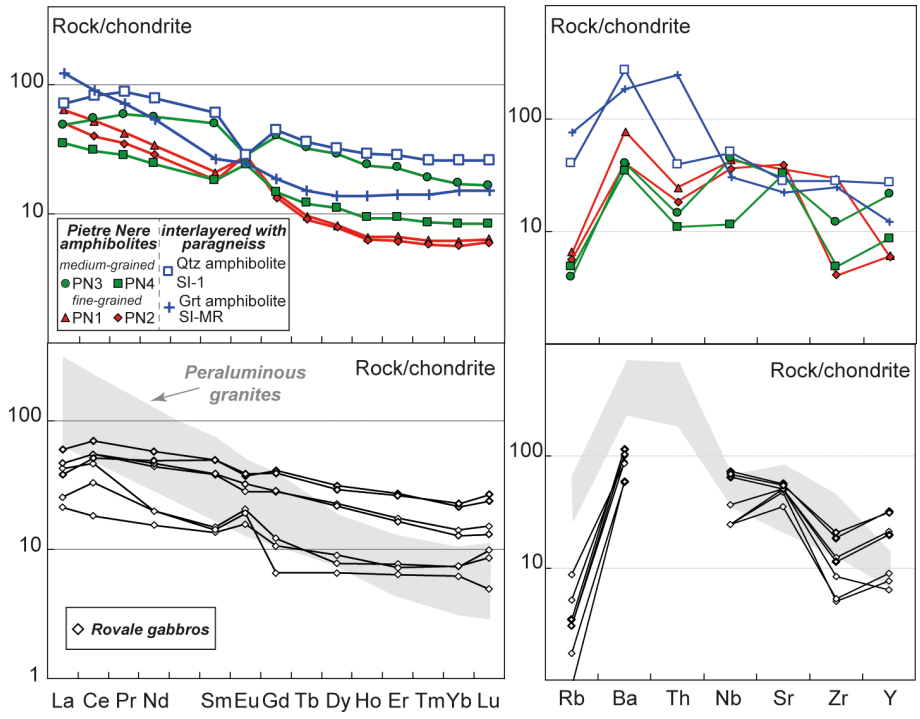

Figure 11. Trace-element whole-rock variation normalized to chondrite (Anders and Ebihara, 1982). The compositions of Rovale gabbros (Sila Massif, Caggianelli et al., 1994) and late-Variscan peraluminous granites (grey field, central and southern Calabria, Rottura et al., 1993; Fiannacca et al., 2019) are reported for comparative purposes.

and Evans, 2010): $\mathrm{Opx} + \mathrm{Qtz} + \mathrm{H_2O} = \mathrm{Cum}$ (Schenk, 1984; Graessner and Schenk, 2001). The Palmi cummingtonite is characterized by high REE contents, with HREEs that are at ~ 10 and ~ 100 times chondrite in the amphibolites from Pietre Nere and interlayered with paragneiss, respectively (Fig. 8). Experimental studies have shown that REEs have a strong preference for silicate melts with respect to aqueous fluids (Adam et al., 2014). I therefore propose that in Palmi amphibolites the crystallization of cummingtonite was produced by the interaction between early crystallized orthopyroxene and a hydrous melt rather than a fluid.

The following reaction for the replacement of orthopyroxene by cummingtonite may be envisaged as follows:

$$\mathrm{Opx} + \mathrm{SiO_2} - \text{rich hydrous melt} = \mathrm{Cum}. \quad \text{(R1)}$$

The proposed cummingtonite-forming reaction implies an open system reactive melt flow, characterized by a coupled dissolution–precipitation process. A similar scenario was proposed for the formation, in the lower and mid crust, of hornblende-rich, hornblendite or biotite-rich rocks by modification of precursor, largely anhydrous gabbroic material (Meek et al., 2019; Piazolo et al., 2020). Cummingtonite formed by replacing precursor orthopyroxene that became unstable, reacted and dissolved in the melt. Coupling of dissolution and precipitation may result in new mineral replacing the volume occupied by the dissolving phase, thereby explaining the local poikilitic habit of amphibole in Pietre Nere amphibolites, which most likely preserves the igneous texture of precursor orthopyroxene. It was indicated that, during high-temperature annealing, the process of dissolution–precipitation may erase microstructures such as interstitial grains with low dihedral angles, commonly related to the presence of migrating melt in a rock (Piazolo et al., 2006, 2020). In Palmi amphibolites, the common occurrence of triple junctions among plagioclase and locally amphibole indicates that annealing could have been responsible for erasing microstructures commonly referred to the presence of a migrating melt.

In Palmi amphibolites, cummingtonite is generally associated with biotite and locally also with allanite (Fig. 4f). The markedly LREE-depleted pattern locally shown by cummingtonite confirms the presence of allanite during cummingtonite formation, because allanite is a REE-rich mineral showing a strong preference of LREEs over HREEs (Fig. 9). Notably, in the Pietre Nere body, the REE pattern of plagioclase from the sample containing allanite is not LREE depleted as the associated cummingtonite but is similar to those of plagioclase from other allanite-free amphibolites (Fig. 9). It suggests that cummingtonite was not at equilibrium with plagioclase, most likely because the duration of heating could have been too short for reaction to go to completion, thereby hindering element diffusion (Vernon, 2004; see also Sect. 6.4). In amphibolites interlayered with paragneiss, both plagioclase and cummingtonite show

LREE-depleted patterns, which indicates that plagioclase crystallized in association with allanite and cummingtonite. Since minor quartz occurs in association with cummingtonite and biotite in amphibolite interlayered with paragneiss, the cummingtonite-forming reaction for Palmi amphibolites may be expressed as follows:

$$\text{Opx}\pm\text{Pl}(1) + \text{SiO}_2 - \text{rich hydrous melt} = \text{Cum} + \text{Bt} \pm \text{Pl}(2) \pm \text{Qtz} \pm \text{Aln}. \quad \text{(R2)}$$

This formulation implies that plagioclase could locally recrystallize simultaneously with the melt–rock reaction. Development of plagioclase after Reaction (R2) may explain the slightly higher anorthite content shown by plagioclase from amphibolites interlayered with paragneiss relative to that from Pietre Nere (Table 2). The incorporation of Ca in Pl (2) could have been also responsible for the minor precipitation of hornblende within amphibolite interlayered with paragneiss (Table 1).

In Palmi amphibolites, cummingtonite is generally rimmed by hornblende (Fig. 4e and g), frequently exhibiting optical continuity, which indicates they form part of a single crystal. Similar hornblende–cummingtonite associations were documented in granulites and amphibolites derived from mafic and ultramafic protoliths (Angus and Kanaris-Sotiriou, 1982; Mongkoltip and Ashworth, 1986; Schenk, 1984). Hornblende (+ quartz) was interpreted to derive by reaction between anorthite-rich plagioclase and cummingtonite, which in turn had formed from precursor orthopyroxene (see also Evans and Ghiorso, 1995). In metabasic rocks from lower-crustal, granulite facies units of the northern Serre from southern Calabria, the derivation of hornblende after cummingtonite was inferred to be coupled with a decrease in the anorthite component in plagioclase (i.e., from An_{90} to An_{70}, Schenk, 1984). Quartz is absent in Pietre Nere amphibolites, which are characterized by the highest modal amounts of hornblende (Table 1), and only occurs in amphibolites interlayered with paragneiss. It is also noteworthy that plagioclase has a relatively homogeneous composition and does not exhibit a decrease in the anorthite content from core to rim, which would be expected in response to the hornblende-producing reaction. I therefore argue that hornblende crystallization after cummingtonite in Palmi amphibolites did not involve a reaction with other minerals.

The envisioned melt–rock reaction initiated with the development of cummingtonite. Following the cummingtonite formation, the reacting melt could enrich in elements having low affinity with respect to cummingtonite, e.g., Ca, Na and Al, which, with decreasing temperature, could promote crystallization of hornblende on cummingtonite. This is consistent with the optically continuity frequently shown by cummingtonite cores to hornblende rims. This hypothesis is also consistent with the increase in REE concentrations from cummingtonite to hornblende because experimental studies for a liquid line of descent of a calc–alkaline basalt at 0.7 GPa determined that amphibole–melt partition coefficients increase systematically with decreasing temperature (Nandedkar et al., 2016); in particular, REE partition coefficients increase up to 1 order of magnitude. Note that the ratios of REEs in hornblende to cummingtonite slightly decrease with an increasing atomic number (Fig. 8), in agreement with a higher compatibility of HREEs relative to LREEs and MREEs in cummingtonite (Tiepolo et al., 2007). Hornblende formation may be thus related to cooling and late-stage crystallization of the migrating melt, incorporating elements that have an extremely low affinity for cummingtonite. The complete reaction for the process leading to the formation of Palmi amphiboles may be schematized as follows:

$$\text{Opx}\pm\text{Pl}(1) + \text{SiO}_2 - \text{rich hydrous melt} = \text{Cum} + \text{Bt} + \text{Hbl} \pm \text{Pl}(2) \pm \text{Qtz} \pm \text{Aln} \pm \text{residual melt}. \quad \text{(R3)}$$

Melt has been included among the reaction products, it could correspond to any melt fraction possibly able to migrate out of the system. The development of amphibole in Palmi amphibolites may be thus attributed to a reaction between precursor orthopyroxene ($\pm$ plagioclase) and a SiO_2-rich hydrous melt, by a coupled dissolution–precipitation process. This reaction was also responsible for the precipitation of biotite $\pm$ allanite $\pm$ quartz $\pm$ plagioclase.

In the Variscan sectors of the Calabria terrane, rocks from the lower crust, after peak metamorphism under granulite facies conditions at 300 ± 10 Ma (U–Pb on zircon and monazite), 790 ± 30 °C and 7.5 ± 0.5 kbar, experienced a nearly isothermal decompression up to 290–280 Ma (Schenk, 1989, 1990; Fornelli et al., 2011). The end of the granulite facies metamorphism was induced by a tectonic event during which the lower crust was uplifted into mid–lower-crust level (~ 5.6 kbar), where it cooled isobarically up to 25 Ma (Schenk, 1990). The temperatures estimated on the basis of hornblende composition for Palmi amphibolites indicate that hornblende crystallization occurred at ~ 800 °C. The two amphiboles show nearly parallel REE patterns with hornblende having higher concentrations levels of about 1 order of magnitude than cummingtonite (Fig. 8). The origin of mineral grains (i.e., clinopyroxene and amphibole) with a similar trace-element variability in gabbros and basalts is commonly attributed to interplay between crystal-growth phenomena and kinetic effects during relatively rapid cooling (e.g., Renna et al., 2011, 2016). It was experimentally shown that at high cooling rates, the crystal growth rate exceeds diffusion rate of components, thereby resulting in the development of a boundary layer at the crystal–melt interface enriched in rejected component (Lofgren et al., 2006; Schwandt and McKay, 2006). I speculate that conditions of relatively rapid crystal growth responsible for hornblende crystallization on cummingtonite rim could be related to the onset of the exhumation and cooling of granulite facies rocks at mid-crustal levels.

6.4 Origin of the garnet amphibolite

Garnet poikiloblast in the amphibolite interlayered with paragneiss contains inclusions of plagioclase and cummingtonite showing variable grain size, rounded to elliptical shape and frequent embayed morphology, thereby indicating that they were partially digested by garnet growth. The idioblastic crystal shape with sharp edges and the inclusion of cummingtonite and anorthite-rich plagioclase (Table 2) that are not present in the neighboring paragneiss (Rochira, 2014) indicate that garnet is not a xenocryst derived from the immediately adjacent migmatites, but it formed in the amphibolite layer.

The embayed morphology of garnet-hosted plagioclase and cummingtonite, in tandem with the absence of plagioclase and cummingtonite in the corona around garnet, suggests that garnet was produced by a reaction involving cummingtonite and plagioclase. The reaction may be referred to that proposed by Hollocher (1991) for Fe-rich metabasic rock in the transitional amphibolite to granulite facies terrane from central Massachusetts (USA): $\mathrm{Cum} + \mathrm{Pl} + \mathrm{Bt} + \mathrm{Ilm} = \mathrm{Hbl} + \mathrm{Grt} + \mathrm{Qtz} + \mathrm{H_2O}$. On the compatibility triangular ACF diagram for metamorphic mafic rocks (Best, 2003) created using the compositions of minerals from the garnet amphibolite, this reaction is confirmed by the intersection between the hornblende–garnet and the anorthite–cummingtonite–biotite tie lines (Fig. S2) agreement with the occurrence of irregularly shaped biotite inclusions in garnet. Hence, quartz included and along the rim of garnet and the rare garnet-hosted hornblende likely formed as a product of a cummingtonite breakdown reaction. The Ca enrichment shown by garnet rim may be attributed to plagioclase breakdown, in agreement with its absence in the corona around the poikiloblast (Fig. 3). Notably, the garnet-forming reaction proposed by Hollocher (1991) implies fluids release and, consequently, their possible interaction with minerals from the matrix. The migration of fluids in the garnet amphibolite is indicated by zircons, which have internal structure characterized by curved patchy pattern and convolute zoning (Fig. 5), commonly related to a reaction with a metamorphic fluid through a coupled dissolution–reprecipitation process (Tomaschek et al., 2003; Geisler et al., 2007; Rubatto et al., 2008). Zircons mostly preserved their euhedral/subhedral habit because the process of dissolution–reprecipitation is inferred to be responsible for the complete replacement of one zircon by another without losing the external shape or crystal morphology of the parent zircon. The numerous inclusions of xenotime in zircons represent another typical sign of their recrystallization because they are generally interpreted to form from the expulsion of non-essential trace elements (i.e., Y and REEs) from the recrystallizing zircons (see also Spandler et al., 2004). It is therefore likely that garnet formed by reaction of cummingtonite + plagioclase + biotite; the garnet-forming reaction was responsible of liberating fluids whose migration was cause for zircon recrystallization.

Garnet poikiloblast shows Mg- and HREE-depleted rim with respect to the core. The lower-Mg zones in garnet rim are most likely the result of diffusive Fe–Mg exchange with the adjacent biotite from the surrounding corona. The HREE-depleted signature of rim to core is consistent with a prograde garnet growth because a progressive decrease in the mass fraction of compatible elements (i.e., Y and HREEs) from core to rim is generally attributed to a Rayleigh-type fractionation process (Otamendi et al., 2002; Rubatto et al., 2020). Subsolidus Fe–Mg and Mg–Mn exchange occurred between garnet and included mafic minerals, as indicated by the higher Mg# and lower MnO shown by cummingtonite within garnet with respect to that in the matrix and the lower $\mathrm{Fe}^{2+}_{\mathrm{tot}}/(\mathrm{Fe}^{2+}_{\mathrm{tot}} + \mathrm{Mg})$ shown by biotite included relative to that in the matrix (Fig. 6; Table 5). Cummingtonite inclusion was also affected by HREE re-equilibration with the host garnet, most likely owing to high-temperature conditions, as indicated by its HREE-depleted pattern with respect to that of cummingtonite in the matrix.

Garnet is absent in the Pietre Nere body and occurs preferentially along the contact between amphibolite layers and migmatites. Smith et al. (2015) showed that metamorphic rocks with heterogeneous texture and mineral abundance may be produced by different extents of reaction and annealing in high-grade gneiss adjacent to intruding plagioclase-rich felsic dikes. The extent of reaction and annealing is greatest in areas adjacent to dike–host boundaries, owing to a long duration of relatively high temperature, whereas further away the reaction is incomplete. This results in an increase in grain size and abundance of reaction products close to the felsic dike. It can be proposed that garnet could develop in amphibolite layers by the cummingtonite–plagioclase–biotite reaction, in close proximity to migmatitic paragneiss, because these could be areas of long durations of high temperatures generated by migmatization and migration of anatectic melts. Exposure to high temperature for a relatively long period may explain the absence in garnet amphibolite of hornblende rim around cummingtonite because its development has been related to conditions of relatively rapid cooling causing rapid crystal growth (see Sect. 6.3). A garnet-forming reaction most likely proceeded in tandem with a high extent of annealing, thereby resulting in the nucleation and growth of coarse-grained garnet. Notably, conditions of a higher extent of annealing in amphibolite interlayered with paragneiss relative to the Pietre Nere body are consistent with evidence for plagioclase recrystallization simultaneously with allanite, amphibole and biotite, namely during the melt–rock reaction process. The Pietre Nere body, further away from the contact with the migmatitic paragneiss, could experience high temperature for a relatively shorter time lapse, which hindered the garnet-forming reaction and was associated with a relatively short time annealing, not

enough for plagioclase recrystallization during the melt–rock reaction.

6.5 Chemical and mineralogical variation in Palmi amphibolites

The amphibolites from Palmi show systematic variations in terms of modal and chemical composition. The highest and lowest amounts of amphibole were found in medium-grained Pietre Nere amphibolites and in amphibolites interlayered within paragneiss, respectively; intermediate amphibole amounts characterize fine-grained Pietre Nere amphibolites (Table 1). Amphibolites interlayered with paragneiss have the highest amounts of biotite, which is minor in fine-grained amphibolites and accessory in medium-grained amphibolites from the Pietre Nere body. Quartz is ~ 7 vol % in amphibolites interlayered within the paragneiss but absent in Pietre Nere amphibolites. The whole rock, cummingtonite and hornblende share a similar variation of Mg#, which increases from the quartz amphibolite to fine- and medium-grained amphibolites of Pietre Nere (Figs. 6, 7 and 10). Furthermore, the $Fe^{2+}_{tot}/(Fe^{2+}_{tot}+Mg)$ of biotite decreases from amphibolites interlayered with paragneiss to fine- and medium-grained Pietre Nere amphibolites (Table 5). Quartz and garnet amphibolites have higher bulk-rock content of K_2O than Pietre Nere amphibolites. Notably hornblende and biotite from amphibolite layers within paragneiss are also enriched in K_2O relative to their counterparts from Pietre Nere, thereby indicating that the K_2O enrichment observed for bulk-rock composition is not related to a low-temperature alteration. A gradual decrease in K_2O-Al_2O_3 and increase in SiO_2 with increasing Mg# is remarkably shown by hornblende compositions (Fig. 7). Moreover, from the amphibolite interlayered with paragneiss to those from Pietre Nere, the contents of MnO in cummingtonite decrease. Major-element variations may be overall explained by a variation in the composition of the reactive migrating melt in response to dissolution of pre-existing minerals and fractionation of new phases. Dissolution of orthopyroxene and crystallization of cummingtonite and biotite could be responsible for the increase in Mg and decrease in Fe in the reactive migrating melt. Biotite fractionation also resulted in a decrease in K_2O and Al_2O_3 of the reacting melt. A decrease in SiO_2 and MnO could reflect the crystallization of quartz and cummingtonite, respectively. The process of reaction, dissolution and precipitation also resulted in an increase in Ca and Na in the migrating melt because these elements are incorporated in negligible amounts in cummingtonite and biotite. Ca and Na enrichment was most likely responsible for a progressive increase in hornblende crystallization as the melt migrated, reacted and crystallized, thereby explaining the increase in hornblende modal amount from the quartz amphibolite to the fine- and medium-grained Pietre Nere amphibolites (Table 1). Hence, the migrating melt could ultimately lead to a predominance of hornblende with respect to cummingtonite in the mineral reaction products.

Mg# of cummingtonite equilibrium melts may be computed assuming amphibole–basalt Fe–Mg partition coefficients of 0.399 as resulting from experiments carried out at 780 °C and 0.7 GPa by Nandedkar et al. (2014). Calculations showed that cummingtonite from the quartz amphibolite, matrix of the garnet amphibolite, fine-grained Pietre Nere amphibolite and medium-grained Pietre Nere amphibolite were in equilibrium with a melt having 29.8, 33.0, 32.7 and 37.2 Mg#, respectively. It was shown that chemical variation of a melt reactively migrating within gabbroic material may be exemplified by a process of assimilation and fractional crystallization (AFC) involving assimilation by the reactively migrating melt of various proportions of pre-existing minerals (e.g., Lissenberg et al., 2013). To simulate whether a melt–rock reaction can reproduce the Mg# of melts at equilibrium with cummingtonite and to discuss the role of the fractionating assemblage I computed an AFC process involving the dissolution of orthopyroxene during the crystallization of the reactively migrating melt. I used the following parameters. (i) The initial melt composition is that of melt in equilibrium with the cummingtonite showing the lowest Mg# (quartz amphibolite). (ii) The model assumes assimilation of orthopyroxene (Ma = 100 % Opx) and crystallization of cummingtonite and biotite. (iii) The composition of assimilated material is that of orthopyroxene from norites of the Variscan Rovale sequence (Sila Massif, Caggianelli et al., 1994). (iv) The partition coefficients used for the AFC are those of Nandedkar et al. (2014). The Mg# of the melt in equilibrium with cummingtonite from fine-grained Pietre Nere amphibolites was reproduced by a fractionating assemblage of 0.35 cummingtonite + 0.65 biotite and an assimilated mass / crystallized mass ratio (Ma/Mc) of 0.85. The Mg# of the melt in equilibrium with cummingtonite from medium-grained Pietre Nere amphibolites was reproduced by a fractionating assemblage of 0.60 cummingtonite + 0.40 biotite and a Ma/Mc ratio of 0.52. It can be thus concluded that modal and major-element variations among Palmi amphibolites reflect an evolution of the reactively migrating melt characterized by variable fractionating assemblage and assimilation to crystallization rates.

Amphibolites are characterized by variable contents of allanite, which is relatively frequent in amphibolites interlayered with paragneiss, but it is rare in the Pietre Nere body where it was only found in foliated fine-grained amphibolite. It is noteworthy that amphibolites interlayered with paragneiss are enriched in most incompatible elements (i.e., Rb, Ba, Th, U) and Zr relative to Pietre Nere samples (Fig. 11). Rb and Ba enrichments are paralleled by cummingtonite and hornblende compositions (Fig. 8). Furthermore, cummingtonite, hornblende and plagioclase from amphibolites interlayered with paragneiss have chondrite-normalized MREE and HREE contents higher by about an order of magnitude than amphibole and plagioclase from Pietre Nere amphibo-

lites. These high concentrations could be related to a high contribution from the reactive migrating melt, which could be also responsible for the high K concentrations shown by the whole rock, hornblende and biotite of amphibolites interlayered with paragneiss. In the Pietre Nere body, fine-grained amphibolites have (i) more fractionated LREE–HREE patterns than medium-grained portions (Fig. 11) and (ii) intermediate Rb_N / Y_N ratios between medium-grained portions and amphibolites interlayered with paragneiss (~ 1.0, ~ 0.4 and 1.5–6.1, respectively, Table S6). It is also noteworthy that foliated fine-grained Pietre Nere amphibolite has both bulk rock and amphibole enriched in Rb and Ba relative to other samples from the Pietre Nere body and Zr bulk-rock contents similar to amphibolites interlayered with paragneiss. These chemical signatures could be related to a higher contribute from the migrating melt in fine-grained relative to medium-grained amphibolites. Hence, allanite abundance and trace-element variations among Palmi amphibolites indicate a decrease in REEs and most incompatible-trace-element contents from amphibolites layers within paragneiss to fine- and medium-grained amphibolites of Pietre Nere. This may reflect a progressive depletion of the migrating melt as it reacts and promotes crystallization of minerals (e.g., amphibole and allanite) able to incorporate a relatively high REE amount and most incompatible elements.

In summary, the reactive melt migration imparted a chemical and mineralogical signature reflecting a variable modification of the protolith initial compositions. In particular, the melt–rock reaction determined an enrichment in SiO_2, Al_2O, K_2O and incompatible elements in amphibolites interlayered with paragneiss relative to those from the Pietre Nere body, most likely promoting the crystallization of minor quartz and relatively high amount of biotite together with amphibole, plagioclase and accessory allanite in rocks in close proximity to migmatites. Within Pietre Nere, foliated fine-grained samples experienced more enrichment in most incompatible elements relative to unfoliated medium-grained amphibolites. Because of its high H_2O contents, the migrating melts could have low viscosity, thereby favoring the process of reactive porous flow (Watson et al., 1990). The chemical and modal variations observed between foliated, fine-grained and unfoliated, medium-grained amphibolites suggest that reactive melt migration was also enhanced by a small grain size and anisotropy, which most likely enabled better interaction with precursor minerals and crystallization of new mineral phases. It is consistent with the AFC computation showing a higher assimilation to crystallization rates in fine-grained relative to medium-grained amphibolites, which implies a higher ability of melt to react with a significant fraction of the host rock (Kelemen, 1986). Textural features could create pressure gradients and permeable pathways facilitating melt migration, as observed for other gabbroic sequences experiencing chemical and mineralogical modification due to a process of deformation-assisted reactive melt migration (Stuart et al., 2018; Meek et al., 2019; Piazolo et al., 2020). On

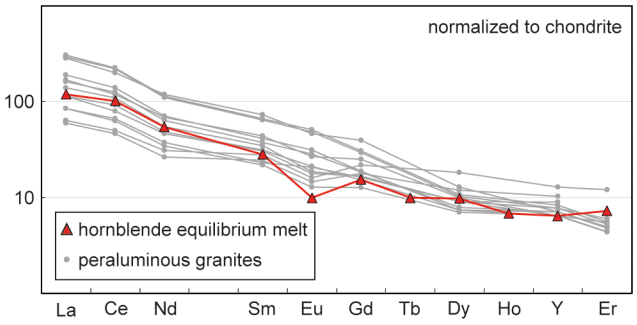

Figure 12. Calculated chondrite-normalized (Anders and Ebihara, 1982) REE and Y compositions of melt in equilibrium with hornblende from fine-grained amphibolite PN2. The amphibole–melt partition coefficients determined experimentally for a melt having $SiO_2 = 63.9$ wt % were used (Nandedkar et al., 2016). $^{Amp/Liq}D$ values are La = 0.329, Ce = 0.714, Nd = 2.334, Sm = 4.19, Eu = 5.052, Gd = 5.43, Tb = 6.062, Dy = 6.041, Ho = 6.46, Y = 6.113 and Er = 5.97. Whole-rock composition of late-Variscan peraluminous granites (Rottura et al., 1993; Fiannacca et al., 2019) are reported for comparative purposes.

the basis of the olivine–basalt partition coefficient reported by Médard and Grove (2008; $K_dOl / basalt^{Fe/Mg} = 0.32$) and orthopyroxene–basalt partition coefficient reported by Müntener et al. (2001; $K_dOpx / basalt^{Fe/Mg} = 0.28$), I calculated Mg# of the melt for the least evolved Rovale gabbros, in order to reduce possible contributes from contamination and/or fractional crystallization. Computed Mg# of the melts in equilibrium with the most primitive olivine and orthopyroxene are 41 and 42, respectively. These values are slightly higher than the Mg# calculated at equilibrium with cummingtonite from medium-grained Pietre Nere amphibolites (~ 37), thereby suggesting that reactive migration of the SiO_2-rich hydrous melt imparted minor chemical variation in these rocks. It can be concluded that fine-grained, foliated rocks represented a high-porosity domain enhancing reactive migration of low viscous hydrous melt and that medium-grained domains could represent a low-porosity barrier possibly preventing further melt migration.

6.6 Inferences on the composition of the migrating melt

The development of biotite, quartz and allanite, in tandem with amphibole, suggests that the reactive migrating melt had a felsic composition. Furthermore, the high MREE and HREE contents and marked negative Sr and Eu anomalies shown by amphibole from amphibolite interlayered with paragneiss indicate that the reacting melt had an evolved trace-element signature (Fig. 8). Notably, the chondrite-normalized patterns of Rb–Ba–Th–Nb–Sr–Zr–Y of quartz and garnet amphibolites nearly coincide with those of late-Variscan, peraluminous granites from central and southern Calabria (Fig. 11). REE compositions of melts in equilibrium with amphiboles from Palmi amphibolites could give

information about the compositions of the reactively migrating melt. Experimental studies support that melt composition, namely SiO_2 content, is the main parameter controlling the absolute values of REE amphibole–melt partition coefficients (Tiepolo et al., 2007; Nandedkar et al., 2016). The SiO_2 content of the parent melt can be inferred based on the major-element mineral chemistry. In particular, the compilation of amphibole compositions by Putirka (2016) allows for calculation of the SiO_2 content of the hornblende equilibrium melt, thereby permitting the choice of suitable amphibole–melt partition coefficients for the system of interest. Calculations indicate that the melts at equilibrium with hornblende had high SiO_2 contents of ~ 60 wt % in the quartz amphibolite, ~ 63 wt % in fine-grained Pietre Nere amphibolites and ~ 68 wt % in medium-grained Pietre Nere amphibolites. Amphiboles whose LREE and MREE compositions were affected by the simultaneous crystallization of allanite (i.e., fine-grained amphibolite PN1 and quartz amphibolite) were not considered for the calculation of equilibrium melts. Hence, REE and Y equilibrium melt compositions were computed using a set of hornblende–melt partition coefficients obtained experimentally for melts having $SiO_2 = 63.9$ wt % (Nandedkar et al., 2016), which is the value obtained for the melt in equilibrium with hornblende from fine-grained amphibolite PN2. Computed REE compositions resemble those of late-Variscan peraluminous granites (Fig. 12). The intrusion in the upper crust of these peraluminous granites was related to a protracted episode of partial melting of lower-crustal metasediments, which started at ~ 300 Ma and ended at ~ 280 Ma (Fiannacca et al., 2008; Micheletti et al., 2008). A whole-rock chemistry and U–Pb zircon dating study recently proposed that the dominant components of the late-Variscan peraluminous granites' magma source was a deep-seated metasediment compositionally similar to migmatitic paragneiss widespread along the southern sector of the Calabria–Peloritani terrane (Fiannacca et al., 2019). A hybrid origin for these granites was also proposed because some of their geochemical and isotopic features may reflect a contribution from mantle-derived components (Rottura et al., 1993). I conclude that the hydrous, SiO_2-rich melt reactively migrating within Palmi mafic rocks had a similar composition to that of late-Variscan peraluminous granites. The reactively migrating melt could derive by partial melting of metasediments akin to neighboring migmatitic paragneiss.

Late-Variscan orogenic collapse of western European Variscides recorded the widespread intrusions of chemically similar basic melts with depleted to slightly enriched isotopic compositions, in different sectors of the original Europe–Adria lithosphere from the crust–mantle boundary (Malenco, Hermann et al., 2001) to the lower crust (e.g., Ivrea Zone, Quick et al., 1994; External Liguride units, Renna and Tribuzio, 2009), mid crust (e.g., Sondalo, Tribuzio et al., 1999; Mont Collon, Monjoie et al., 2005) and shallow crust (Corsica batholith, Renna et al., 2007; Tribuzio et al., 2009). These intrusions were dated from ~ 306 to ~ 280 Ma and were associated with lithosphere thinning/extension and uprise of asthenospheric mantle. The emplacement of gabbroic sequences of western European Variscides was nearly coeval with the proposed late-Variscan intrusions of mantle-derived magmas in several sectors of the Calabria terrane (e.g., Caggianelli et al., 1994; Renna et al., 2020). In a geodynamic scenario characterized by lithospheric extension and attenuation subsequent to the Variscan collision, high heat input from the rising mantle could have contributed to producing partial melting of lower-crust metasedimentary rocks.

7 Summary and concluding remarks

This work deals with a portion of the Variscan lower to intermediate crust exposed in the Palmi area (southwestern Calabria, Italy). Amphibolites occur in close spatial relationship with migmatitic paragneiss, namely as decimeter-thick layers within the migmatites and as a decametric main body (i.e., Pietre Nere body) adjacent to the paragneiss. The decametric body is mainly fine-grained and weakly to moderately foliated; unfoliated medium-grained portions also rarely occur.

Amphibolites derived from mafic rocks of cumulus origin. Amphibole development likely resulted from a coupled dissolution–precipitation process as a consequence of the reaction between a migrating SiO_2-rich hydrous melt and precursor orthopyroxene. This reaction was also responsible for the crystallization of biotite $\pm$ allanite $\pm$ quartz $\pm$ plagioclase and most likely occurred in conjunction with a subsolidus re-equilibration under granulite facies conditions. The SiO_2-rich hydrous melt had a similar composition to that of late-Variscan peraluminous granites and could derive by partial melting of metasediments akin to neighboring migmatitic paragneiss. Garnet formed by reaction between cummingtonite, plagioclase and biotite in amphibolites interlayered with paragneiss, most likely due to relatively long period of high temperatures generated by anatexis.

This study provides evidence that reactive migmatite-related melt migration is a viable mechanism by which major and trace elements are transferred from the anatectic source to adjacent mafic rocks. The melt–rock reaction promoted amphibole and accessory mineral (i.e., allanite) crystallization, which played an important role in the distribution of most incompatible trace elements and REEs during the migration of migmatite-related melt in mafic crust out of the anatectic source. The reactive migration of the melt imparted a mineralogical and chemical signature in mafic rocks, which reflects an increasing modification of the original compositions with proximity to migmatites. The effects of the reactive melt migration were enhanced in fine-grained, foliated rocks which could represent a high-porosity domain enabling better interaction with precursor minerals and nucleation of new mineral phases. Medium-grained domains preserved compositions more similar to pristine mafic rocks and

could represent a low-porosity barrier possibly preventing further melt migration.

Data availability. All data derived from this research are presented in the enclosed figures and tables.

Supplement. The supplement related to this article is available online at: https://doi.org/10.5194/ejm-35-1-2023-supplement.

Competing interests. The author has declared that there are no competing interests.

Disclaimer. Publisher's note: Copernicus Publications remains neutral with regard to jurisdictional claims in published maps and institutional affiliations.

Acknowledgements. Antonio Langone, Giacomo Prosser and Alfredo Caggianelli are thanked for constructive discussions. Antonio Langone is also thanked for support in mineral trace-element analyses carried out at the CNR IGG UOS of Pavia. I thank reviewers Silvio Ferrero and Gerhard Franz and editors Elisabetta Rampone and Klaus Mezger for their thorough evaluations and stimulating comments, which considerably improved the quality of this study.

Financial support. The research was financially supported by FFABR (Finanziamento Attività di Base della Ricerca di Ateneo) Unime 2019 and 2021 of the Università degli Studi di Messina.

Review statement. This paper was edited by Klaus Mezger and reviewed by Silvio Ferrero and Gerhard Franz.

References

Adam, J., Locmelis, M., Afonso, J. C., Rushmer, T., and Fiorentini, M. L.: The capacity of hydrous fluids to transport and fractionate incompatible elements and metals within the Earth's mantle, Geochem. Geophy. Geosy., 15, 2241–2253, 2014.

Alessio, K. L., Hand, M., Kelsey, D. E., Williams, M. A., Morrissey, L. J., and Barovich, K.: Conservation of deep crustal heat production, Geology, 46, 335–338, 2018.

Alvarez, W., Cocozza, T., and Wezel, F. C.: Fragmentation of the Alpine orogenic belt by microplate dispersal, Nature, 248, 309–314, 1974.

Amodio-Morelli, L., Bonardi, G., Colonna, V., Dietrich, D., Giunta, G., Ippolito, F., Liguori, V., Lorenzoni, S., Paglionico, A., Perrone, V., Piccarreta, G., Russo, M., Scandone, P., Zanettin-Lorenzoni, E., and Zuppetta, A.: L'Arco Calabro – Peloritano nell'orogene appenninico-maghrebide, Mem. Soc. Geol. Ital., 17, 1–60, 1976.

Anders, E. and Ebihara, M.: Solar-system abundances of the elements, Geochim. Cosmochim. Ac., 46, 2363–2380, 1982.

Angus, N. S. and Kanaris-Sotiriou, R.: Autometasomatic gneisses of the Currywongaun-Doughruagh syntectonic intrusion, Connemara Ireland, Mineral. Mag., 46, 411–420, 1982.

Ayuso, R. A., Messina, A., De Vivo, B., Russo, S., Woodruff, L. G., Sutter, J. F., and Belkin, H. E.: Geochemistry and argon thermochronology of the Variscan Sila Batholith, southern Italy: source rocks and magma evolution, Contrib. Mineral. Petr., 117, 87–109, 1994.

Best, M. G.: Igneous and metamorphic petrology, (Second Edition), Blackwell Publishing, Oxford, ISBN 1-40510-588-7, 2003.

Bea, F.: Controls on the trace element composition of crustal melts, Earth Env. Sci. T. R. So, 87, 33–41, 1996.

Bonardi, G., Cavazza, W., Perrone, V., and Rossi, S.: Calabria-Peloritani terrane and northern Ionian sea. In Anatomy of an orogen: The Apennines and adjacent Mediterranean basins, Springer, Dordrecht, 287–306, 2001.

Brown, M., Korhonen, F. J., and Siddoway, C. S.: Organizing melt flow through the crust, Elements, 7, 261–266, 2011.

Caggianelli, A. and Di Florio, M. R.: Trondhjemitic evolution caused by compaction of a crystal mush: an example from southern Calabria (Italy), Period. Mineral., 58, 9–23, 1989.

Caggianelli, A., Moro, A. D., and Piccarreta, G.: Petrology of basic and intermediate orogenic granitoids from the Sila Massif (Calabria, southern Italy), Geol. J., 29, 11–28, 1994.

Caggianelli, A., Prosser, G., and Di Battista, P.: Textural features and fabric analysis of granitoids emplaced at different depths: the example of the Hercynian tonalites and granodiorites from Calabria, Mineralogica and Petrographica Acta, 40, 11–26, 1997.

Caggianelli, A., Moro, A. D., Di Battista, P., Prosser, G., and Rottura, A.: Leucogranite genesis connected with low-pressure high-temperature metamorphism in the Sila basement (Calabria, Italy), Swiss Bulletin of Mineralogy and Petrology, 83, 301–316, 2003.

Caggianelli, A., Prosser, G., Festa, V., Langone, A., and Spiess, R.: GFT-Geological Field Trips. In Congresso Nazionale della Società Geologica Italiana-Arcavacata di Rende (CS), 18, p. 20, 2012.

Deering, C. D., Cole, J. W., and Vogel, T. A.: A rhyolite compositional continuum governed by lower crustal source conditions in the Taupo Volcanic Zone, New Zealand, J. Petrol., 49, 2245–2276, 2008.

Dubois, R.: Definition d'un socle antehercynien en Calabre, Comptes Rendus Academie des Sciences de Paris, 272, 2052–2055, 1971.

Elburg, M. A.: Evidence of isotopic equilibration between microgranitoid enclaves and host granodiorite, Warburton Granodiorite, Lachlan Fold Belt, Australia, Lithos, 38, 1–22, 1996.

Evans, B. W. and Ghiorso, M. S.: Thermodynanics and petrology of cummingtonite, Am. Mineral., 80, 649–663, 1995.

Festa, V., Langone, A., Caggianelli, A., and Rottura, A.: Dike magmatism in the Sila Grande (Calabria, southern Italy): evidence of Pennsylvanian–Early Permian exhumation, Geosphere, 6, 549–566, 2010.

Festa, V., Prosser, G., Caggianelli, A., Grande, A., Langone, A., and Mele, D.: Vorticity analysis of the Palmi shear zone mylonites: new insights for the Alpine tectonic evolution of the Calabria–Peloritani terrane (southern Italy), Geol. J., 51, 670–681, 2015.

Fiannacca, P., Williams, I. S., Cirrincione, R., and Pezzino, A.: Crustal contributions to late Hercynian peraluminous magmatism in the southern Calabria–Peloritani Orogen, southern Italy: petrogenetic inferences and the Gondwana connection, J. Petrol., 49, 1497–1514, 2008.

Fiannacca, P., Williams, I. S., Cirrincione, R., and Pezzino, A.: Poly-orogenic melting of metasedimentary crust from a granite geochemistry and inherited zircon perspective (Southern Calabria-Peloritani Orogen, Italy), Front. Earth Sci., 7, 119, https://doi.org/10.3389/feart.2019.00119, 2019.

Fornelli, A., Langone, A., Micheletti, F., and Piccarreta, G.: Time and duration of Variscan high-temperature metamorphic processes in the south European Variscides: constraints from U-Pb chronology and trace element chemistry of zircon, Miner. Petrol., 103, 101–122, 2011.

Geisler, T., Schaltegger, U., and Tomaschek, F.: Re-equilibration of zircon in aqueous fluids and melts, Elements, 3, 43–50, 2007.

Geschwind, C. H. and Rutherford, M. J.: Cummingtonite and the evolution of the Mount St. Helens (Washington) magma system: an experimental study, Geology, 20, 1011–1014, 1992.

Graessner, T. and Schenk, V.: An exposed Hercynian deep crustal section in the Sila Massif of northern Calabria: mineral chemistry, petrology and a P–T path of granulite-facies metapelitic migmatites and metabasites, J. Petrol., 42, 931–961, 2001.

Graessner, T., Schenk, V., Bröcker, M., and Mezger, K.: Geochronological constraints on the timing of granitoid magmatism, metamorphism and post-metamorphic cooling in the Hercynian crustal cross-section of Calabria, J. Metamorph. Geol., 18, 409–421, 2000.

Grande, A., Di Vincenzo, G., Prosser, G., and Caggianelli, A.: Direct evidence of Middle Oligocene extension in the Calabria–Peloritani terrane from co-seismic faulting: the pseudotachylyte-bearing shear zones of Palmi (southern Calabria, Italy), Terra Nova, 21, 293–303, 2009.

Hawthorne, F. C., Oberti, R., Harlow, G. E., Maresch, W. V., Martin, R. F., Schumacher, J. C., and Welch, M. D.: Nomenclature of the amphibole supergroup, Am. Mineral., 97, 2031–2048, 2012.

Hermann, J., Müntener, O., and Günther, D.: Differentiation of mafic magma in a continental crust-to-mantle transition zone, J. Petrol., 42, 189–206, 2001.

Holland, T. and Blundy, J.: Non-ideal interactions in calcic amphiboles and their bearing on amphibole-plagioclase thermometry, Contrib. Mineral. Petr., 116, 433–447, 1994.

Hollocher, K.: Prograde amphibole dehydration reactions during high-grade regional metamorphism, central Massachusetts, USA. Am. Mineral., 76, 956–970, 1991.

Kelemen, P. B.: Assimilation of ultramafic rock in subduction-related magmatic arcs, J. Geol., 94, 829–843, 1986.

Kempton, P. D. and Harmon, R. S.: Oxygen isotope evidence for large-scale hybridization of the lower crust during magmatic underplating, Geochim. Cosmochim. Ac., 56, 971–986, 1992.

Langone, A., Caggianelli, A., Festa, V., and Prosser, G.: Time constraints on the building of the Serre Batholith: consequences for the thermal evolution of the Hercynian continental crust exposed in Calabria (southern Italy), J. Geol., 122, 183–199, 2014.

Lissenberg, C. J., MacLeod, C. J., Howard, K. A., and Godard, M.: Pervasive reactive melt migration through fast-spreading lower oceanic crust (Hess Deep, equatorial Pacific Ocean), Earth Planet. Sc. Lett., 361, 436–447, 2013.

Lofgren, G. E., Huss, G. R., and Wasserburg, G. J.: An experimental study of trace-element partitioning between Ti-Al-clinopyroxene and melt: Equilibrium and kinetic effects including sector zoning, Am. Mineral., 91, 1596–1606, 2006.

Médard, E. and Grove, T. L.: The effect of H_2O on the olivine liquidus of basaltic melts: experiments and thermodynamic models, Contrib. Mineral. Petr., 155, 417–432, 2008.

Meek, U., Piazolo, S., and Daczko, N. R.: The field and microstructural signatures of deformation-assisted melt transfer: Insights from magmatic arc lower crust, New Zealand, J. Metamorph. Geol., 37, 795–821, 2019.

Micheletti, F., Fornelli, A., Piccarreta, G., Barbey, P., and Tiepolo, M.: The basement of Calabria (southern Italy) within the context of the Southern European Variscides: LA-ICPMS and SIMS U–Pb zircon study, Lithos, 104, 1–11, 2008.

Mongkoltip, P. and Ashworth, J. R.: Amphibolitization of metagabbros in the Scottish Highlands, J. Metamor. Geol., 4, 261–283, 1986.

Monjoie, P., Bussy, F., Lapierre, H., and Pfeifer, H. R.: Modeling of in-situ crystallization processes in the Permian mafic layered intrusion of Mont Collon (Dent Blanche nappe, western Alps), Lithos, 83, 317–346, 2005.

Mottana, A., Bocchio, R., Crespi, R., De Capitani, L., Liborio, G., and Della Ventura, G.: Cummingtonite in the amphibolites of the South-Alpine Basement Complex (Upper Lake Como region, Italy): its relationships with hornblende, Miner. Petrol., 51, 67–84, 1994.

Müntener, O., Kelemen, P. B., and Grove, T. L.: The role of H_2O during crystallization of primitive arc magmas under uppermost mantle conditions and genesis of igneous pyroxenites: an experimental study, Contrib. Mineral. Petr., 141, 643–658, 2001.

Nandedkar, R. H., Ulmer, P., and Müntener, O.: Fractional crystallization of primitive, hydrous arc magmas: an experimental study at 0.7 GPa, Contrib. Mineral. Petr., 167, 1–27, 2014.

Nandedkar, R. H., Hürlimann, N., Ulmer, P., and Müntener, O.: Amphibole–melt trace element partitioning of fractionating calc-alkaline magmas in the lower crust: an experimental study, Contrib. Mineral. Petr., 171, 1–25, 2016.

Otamendi, J. E., de La Rosa, J. D., Douce, A. E. P., and Castro, A.: Rayleigh fractionation of heavy rare earths and yttrium during metamorphic garnet growth, Geology, 30, 159–162, 2002.

Piazolo, S., Bestmann, M., Prior, D. J., and Spiers, C. J. Temperature dependent grain boundary migration in deformed-then-annealed material: observations from experimentally deformed synthetic rocksalt, Tectonophysics, 427, 55–71, 2006.

Piazolo, S., Daczko, N. R., Silva, D., and Raimondo, T.: Melt-present shear zones enable intracontinental orogenesis, Geology, 48, 643–648, 2020.

Pin, C. and Vielzeuf, D.: Granulites and related rocks in Variscan median Europe: a dualistic interpretation, Tectonophysics, 93, 47–74, 1983.

Prosser, G., Caggianelli, A., Rottura, A., and Del Moro, A.: Strain localisation driven by marble layers: the Palmi shear zone (Calabria-Peloritani terrane, southern Italy), GeoActa, 2, 155–166, 2003.

Putirka, K.: Amphibole thermometers and barometers for igneous systems and some implications for eruption mechanisms of felsic magmas at arc volcanoes, Am. Mineral., 101, 841–858, 2016.

Quick, J. E., Sinigoi, S., and Mayer, A.: Emplacement dynamics of a large mafic intrusion in the lower crust, Ivrea-Verbano Zone, northern Italy, J. Geophys. Res.-Sol. Ea., 99, 21559–21573, 1994.

Reichardt, H. and Weinberg, R. F.: Hornblende chemistry in meta- and diatexites and its retention in the source of leucogranites: an example from the Karakoram Shear Zone, NW India, J. Petrol., 53, 1287–1318, 2012.

Renna, M. R. and Tribuzio, R.: Petrology, geochemistry and U–Pb zircon geochronology of lower crust pyroxenites from northern Apennine (Italy): insights into the post-collisional Variscan evolution, Contrib. Mineral. Petr., 157, 813–835, 2009.

Renna, M. R., Tribuzio, R., and Tiepolo, M.: Origin and timing of the post-Variscan gabbro–granite complex of Porto (Western Corsica), Contrib. Mineral. Petr., 154, 493–517, 2007.

Renna, M. R., Tiepolo, M., and Tribuzio, R.: In situ U-Pb geochronology of baddeleyite-zircon pairs using laser-ablation ICPMS: the case-study of quartz gabbro from Varney Nunatak (central Victoria Land, Antarctica), Eur. J. Mineral., 23, 223–240, 2011.

Renna, M. R., Tribuzio, R., and Ottolini, L.: New perspectives on the origin of olivine-rich troctolites and associated harrisites from the Ligurian ophiolites (Italy), J. Geol. Soc., 173, 916–932, 2016.

Renna, M. R., Langone, A., Caggianelli, A., and Prosser, G.: Chemical signature of migmatite-related melts migration in lower mafic crust: mineral geochemistry and zircon dating constraints (Variscan lower crust, SW Calabria, Italy), EGU General Assembly 2020, Online, 4–8 May 2020, EGU2020-7029, https://doi.org/10.5194/egusphere-egu2020-7029, 2020.

Roberts, M. P., Pin, C., Clemens, J. D., and Paquette, J. L.: Petrogenesis of mafic to felsic plutonic rock associations: the calc-alkaline Quérigut complex, French Pyrenees, J. Petrol., 41, 809–844, 2000.

Rochira, F.: Processi di fusione parziale nella crosta continentale inferiore: le migmatiti dello Scoglio dell'Isola (Palmi, Calabria), MS thesis, University of Bari, 2014.

Rottura, A.: The tonalitic gneisses from Palmi-Bagnara, Calabrian Arc (Southern Italy): geochemistry, their protholits, and tectono-metamorphic evolution, Neues Jahrb. für Mineral. Abhandlungen, 152, 187–210, 1985.

Rottura, A., Bargossi, G. M., Caironi, V., Del Moro, A., Maccarrone, E., Macera, P., Paglionico, A., Petrini, R., Piccarreta, G., and Poli, G.: Petrogenesis of contrasting Hercynian granitoids from the Calabrian Arc, southern Italy, Lithos, 24, 97–119, 1990.

Rottura, A., Caggianelli, A., Campana, R., and Del Moro, A.: Petrogenesis of Hercynian peraluminous granites from the Calabrian Arc, Italy, Eur. J. Mineral., 5, 737–754, 1993.

Rubatto, D., Müntener, O., Barnhoorn, A., and Gregory, C.: Dissolution-reprecipitation of zircon at low-temperature, high-pressure conditions (Lanzo Massif, Italy), Am. Mineral., 93, 1519–1529 2008.

Rubatto, D., Burger, M., Lanari, P., Hattendorf, B., Schwarz, G., Neff, C., Schmidt, P. K., Hermann, J., Vho, A., and Günther, D.: Identification of growth mechanisms in metamorphic garnet by high-resolution trace element mapping with LA-ICP-TOFMS, Contrib. Mineral. Petr., 175, 1–19, 2020.

Sanfilippo, A., MacLeod, C. J., Tribuzio, R., Lissenberg, C. J., and Zanetti, A.: Early-stage melt-rock reaction in a cooling crystal mush beneath a slow-spreading mid-ocean ridge (IODP Hole U1473A, Atlantis Bank, Southwest Indian Ridge), Front. Earth Sci., 8, 579138, https://doi.org/10.3389/feart.2020.579138, 2020.

Sawyer, E. W.: Disequilibrium melting and the rate of melt–residuum separation during migmatization of mafic rocks from the Grenville Front, Quebec, J. Petrol., 32, 701–738, 1991.

Sawyer, E. W., Cesare, B., and Brown, M.: When the continental crust melts, Elements, 7, 229–234, 2011.

Schwandt, C. S. and McKay, G. A.: Minor-and trace-element sector zoning in synthetic enstatite, Am. Mineral., 91, 1607–1615, 2006.

Schenk, V.: U-Pb and Rb-Sr radiometric dates and their correlation with metamorphic events in the granulite-facies basement of the Serre, southern Calabria (Italy), Contrib. Mineral. Petr., 73, 23–38, 1980.

Schenk, V.: Petrology of felsic granulites, metapelites, metabasics, ultramafics, and metacarbonates from Southern Calabria (Italy): prograde metamorphism, uplift and cooling of a former lower crust, J. Petrol., 25, 255–296, 1984.

Schenk, V.: PTt path of the lower crust in the Hercynian fold belt of southern Calabria, Geol. Soc., London, Special Publications, 43, 337–342, 1989.

Schenk, V.: The exposed crustal cross section of southern Calabria, Italy: structure and evolution of a segment of Hercynian crust, in: Exposed cross-sections of the continental crust, Springer, Dordrecht, 21–42, 1990.

Schumacher, J. C.: Metamorphic amphiboles: composition and coexistence, Rev. Mineral. Geochem., 67, 359–416, 2007.

Schwindinger, M., Weinberg, R. F., and White, R. W.: The fate of accessory minerals and key trace elements during anatexis and magma extraction, J. Petrol., 61, egaa031, https://doi.org/10.1093/petrology/egaa031, 2020.

Smith, J. R., Piazolo, S., Daczko, N. R., and Evans, L.: The effect of pre-tectonic reaction and annealing extent on behaviour during subsequent deformation: Insights from paired shear zones in the lower crust of Fiordland, New Zealand, J. Metamorph. Geol., 33, 557–577, 2015.

Spandler, C., Hermann, J., and Rubatto, D.: Exsolution of thortveitite, yttrialite, and xenotime during low-temperature recrystallization of zircon from New Caledonia, and their significance for trace element incorporation in zircon, Am. Mineral., 89, 1795–1806, 2004.

Stuart, C. A., Piazolo, S., and Daczko, N. R.: The recognition of former melt flux through high-strain zones, J. Metamorph. Geol., 36, 1049–1069, 2018.

Tiepolo, M., Oberti, R., Zanetti, A., Vannucci, R., and Foley, S. F.: Trace-element partitioning between amphibole and silicate melt, Rev. Mineral. Geochem., 67, 417–452, 2007.

Tomaschek, F., Kennedy, A. K., Villa, I. M., Lagos, M., and Ballhaus, C.: Zircons from Syros, Cyclades, Greece–recrystallization and mobilization of zircon during high-pressure metamorphism, J. Petrol., 44, 1977–2002. 2003.

Tribuzio, R., Thirlwall, M. F., and Messiga, B.: Petrology, mineral and isotope geochemistry of the Sondalo gabbroic complex (Central Alps, Northern Italy): implications for the origin of post-Variscan magmatism, Contrib. Mineral. Petr., 136, 48–62, 1999.

Tribuzio, R., Renna, M. R., Braga, R., and Dallai, L.: Petrogenesis of Early Permian olivine-bearing cumulates and associated basalt

dykes from Bocca di Tenda (Northern Corsica): implications for post-collisional Variscan evolution, Chem. Geol., 259, 190–203, 2009.

Vernon, R. H.: Microstructures of deformed rocks, A practical guide to rock microstructure, Cambridge University Press, Cambridge, 295–474, 2004.

Watson, B. E., Brenan, J. M., and Baker, D. R.: Distribution of fluids in the continental mantle, in: Continental mantle, edited by: Menzies, M. A., Clarendon Press, Oxford, 111–125, 1990.

Whitney, D. L. and Evans, B. W.: Abbreviations for names of rock-forming minerals, Am. Mineral., 95, 185–187, 2010.

Wolfram, L. C., Weinberg, R. F., Hasalová, P., and Becchio, R.: How melt segregation affects granite chemistry: Migmatites from the Sierra de Quilmes, NW Argentina, J. Petrol., 58, 2339–2364, 2017.